A partitioned Newton method for the interaction of a fluid and a 3D shell structure

Miguel Angel Fernández, Jean-Frédéric Gerbeau, Antoine Gloria, Marina Vidrascu

INRIA

INSTITUT NATIONAL DE RECHERCHE EN INFORMATIQUE ET EN AUTOMATIQUE

A partitioned Newton method for the interaction of a fluid and a 3D shell structure

Miguel A. Fernández — Jean-Frédéric Gerbeau — Antoine Gloria — Marina Vidrascu

N° 6623

August 2008

Thèmes BIO et NUM

ISSN 0249-6399 ISRN INRIA/RR--6623--FR+ENG

INSTITUT NATIONAL
DE RECHERCHE
EN INFORMATIQUE
ET EN AUTOMATIQUE

INRIA

centre de recherche
PARIS - ROCQUENCOURT

A partitioned Newton method for the interaction of a fluid and a 3D shell structure

Miguel A. Fernández* , Jean-Frédéric Gerbeau† , Antoine Gloria‡ , Marina Vidrascu§

Thèmes BIO et NUM — Systèmes biologiques et Systèmes numériques
Équipes-Projets REO & MACS

Rapport de recherche n° 6623 — August 2008 — 30 pages

Abstract: We review various fluid-structure algorithms based on domain decomposition techniques and we propose a new one. The standard methods used in fluid-structure interaction problems are generally "nonlinear on subdomains". We propose a scheme based on the principle "linearize first, then decompose". In other words we extend to fluid-structure problems domain decomposition techniques classically used in nonlinear elasticity.

Key-words: fluid-structure interaction, Newton algorithm, nonlinear domain decomposition, 3D shell

* Project-team REO, INRIA Paris-Rocquencourt & Paris 6 University
† Project-team REO, INRIA Paris-Rocquencourt & Paris 6 University
‡ Project-teams MICMAC & REO, ENPC & INRIA Paris-Rocquencourt
§ Project-team MACS, INRIA Paris-Rocquencourt

Centre de recherche INRIA Paris – Rocquencourt
Domaine de Voluceau, Rocquencourt, BP 105, 78153 Le Chesnay Cedex
Téléphone : +33 1 39 63 55 11 — Télécopie : +33 1 39 63 53 30

Une méthode de Newton partionnée pour l'interaction d'un fluide et d'une coque 3D

Résumé : Nous faisons une revue de divers algorithmes de couplage fluide-structure basés sur des techniques de décomposition de domaine et nous en proposons un nouveau. Les méthodes classiques utilisées en interaction fluide-structure sont généralement "non linéaires par sous-domaine". Nous proposons un schéma basé sur le principe "linéariser puis décomposer". En d'autres termes, nous étendons aux problèmes d'interaction fluide-structure des techniques de décomposition de domaine utilisées classiquement en élasticité non linéaire.

Mots-clés : interaction fluide-structure, algorithme de Newton, décomposition de domaine non linéaire, coque 3D

Introduction

In this paper we review various numerical methods to treat the interaction between an incompressible fluid and an elastic structure, and we propose a new approach based on a Newton algorithm and domain decomposition methods. To model the structure, we use 3D-shell elements, which allows us to use three dimensional constitutive laws (see [10, 12, 11]). Up to our knowledge, this is the first time such elements are used in fluid-structure interaction.

Fluid-structure algorithms are too numerous to be reviewed exhaustively. A classification of the various approaches is not obvious either. To begin with, we can consider two groups of methods: the "strongly coupled" and the "loosely coupled" schemes. This distinction is quite clear since it corresponds to a precise property: those schemes which can ensure a well-balanced energy transfer between the fluid and the structure can be called "strongly coupled", the other ones are "loosely coupled". All the methods presented in this study are strongly coupled. Loosely coupled schemes, which are very powerful in many applications but can be unstable in others, are not considered here. We refer for example to [41, 18, 6] for explicit coupling schemes and to [19, 20] for a semi-implicit coupling scheme.

We can then distinguish "monolithic" and "partitioned" schemes. For example, an *ad hoc* solver whose purpose is to solve simultaneously the fluid and the structure typically leads to a monolithic scheme (see [42, 45, 48, 28, 2, 30, 16, 5], for instance). On the other hand, coupling one fluid solver and one structure solver as black boxes clearly yields a partitioned scheme. Such a partitioned scheme can be strongly coupled as soon as sub-iterations are performed at each time step. The number of subiterations being very large in some application, acceleration techniques have been investigated in several articles: for example Le Tallec and Mouro [33] propose a steepest descent approach, Mok *et al.* [38] (see also [31]) propose an Aitken acceleration which is based on the two previously computed solutions, Vierendeels [47] a least-square method which uses several previously computed solutions, and Badia *et al.* [1] an specific linear combination of the coupling conditions.

It is well-known, in particular since the work by Le Tallec and Mouro [33] and more recently by Deparis *et al.* [15, 14], that fluid-structure problems can be tackled with domain decomposition approaches. Indeed, a fluid-structure problem can be viewed as a general continuum mechanics problem set on one domain which is split into a fluid part and a structure part. The fluid-structure coupling conditions then appear as the transmission conditions which ensure that the solution of the global problem is obtained by "sticking" the two subproblem solutions. This point of view has been adopted in various studies, either with the so-called "Dirichlet-Neumann" algorithms (see for example [36, 26, 23]) or with "Neumann-Neumann" algorithms ([15, 14]).

All these methods have been devised following the rule "apply domain decomposition to the nonlinear global problem and then solve on each subdomain the nonlinear problems". On the contrary, in other fields – for example nonlinear elasticity [32] – domain decomposition is usually applied with the rule "linearize first, then solve the tangent problem using domain decomposition". The purpose of this paper is to propose a fluid-structure algorithm based on the last rule. The resulting algorithm can be viewed as a monolithic scheme in the sense that we apply a Newton algorithm to the global fluid-structure

problem. But, it is more conform to the practical implementation to consider it as a partitioned scheme, since the fluid and the structure are solved with two different solvers, with their own schemes, and can be run in parallel. Contrarily to the methods following the first rule, these solvers are only used to solve the tangent problems and to evaluate nonlinear residuals. The use of two different solvers has well-known advantages (re-usability of existing codes, flexible choice of the numerical methods adapted to each sub-problem, *etc.*). Compared to monolithic schemes presented in the literature [42, 45, 48, 28, 2, 30, 16, 5], our approach may have another advantage: the use of domain decomposition methods to solve the tangent problem is expected to be more efficient than direct methods or iterative methods based on block-preconditioners.

The remainder of the paper is organized as follows. In Section 1 we review some standard approaches to solve fluid-structure interaction problems, in particular those based on domain decomposition arguments, that use the so-called Steklov-Poincaré operators. In Section 2 we recall the fluid and solid models and we set the main notations. In Section 3 we propose a short review on constitutive laws that have been developed recently to model soft tissues, and in particular the arterial wall. The development of constitutive laws for soft tissues is of interest from the numerical point of view. On the one hand, specific features of the model can lead to specific numerical issues such as locking (incompressibility, thin three dimensional structures) and will motivate the use of 3D shell elements. On the other hand, the change of relative complexity of the structure with respect to the fluid can change the relative efficiency of a method with respect to another one. The time scheme is presented in Section 4. In Section 5 the new algorithm is introduced. We propose in Section 5.3 a simplified complexity analysis in which compare the efficiency of the proposed algorithm with other existing approaches. We propose in Section 5.3 a simplified complexity analysis whose conclusion may be sum up as follows: the more expensive the structure problem and nonlinear the fluid (let think of the Navier-Stokes equations but also of complex models for the fluid), the more competitive is expected this new formulation. Numerical results and a comparison with existing methods are reported in Section 6. Finally, some conclusions are given in Section 7.

1 Classical solution methods

In this section, we briefly review some of the existing algorithms for the numerical solution of the nonlinear system arising in the time discretization of the fluid-structure problem with an implicit coupling scheme. These methods are typically based on the application of a particular nonlinear iterative method to three different formulations of the nonlinear coupled system.

In general, the time discretization of a fluid-structure problem with an implicit coupling scheme leads to a coupled nonlinear problem of the type: Find the interface displacement $\boldsymbol{\gamma}$, the fluid state $\boldsymbol{x}_f$ and the solid state $\boldsymbol{x}_s$ such that

$$\text{Formulation (I):} \qquad \begin{cases} \mathcal{F}\left(\boldsymbol{x}_f, \boldsymbol{\gamma}\right) = 0, \\ \mathcal{S}\left(\boldsymbol{x}_s, \boldsymbol{\gamma}\right) = 0, \\ \mathcal{I}\left(\boldsymbol{x}_f, \boldsymbol{x}_s\right) = 0. \end{cases} \tag{1}$$

Equations $(1)_1$ and $(1)_2$ ensure the equilibrium of momentum when the fluid and the solid are subjected to an interface displacement $\boldsymbol{\gamma}$, whereas the last equation enforces the equilibrium of mechanical stresses at the interface.

Problem (1) can be reformulated in terms of $\boldsymbol{\gamma}$ by eliminating the fluid and solid unknowns $\boldsymbol{x}_f, \boldsymbol{x}_s$. This yields to the so-called Steklov-Poincaré formulation: Find the interface displacement $\boldsymbol{\gamma}$ such that,

$$\text{Formulation (II):} \qquad S_f(\boldsymbol{\gamma}) + S_s(\boldsymbol{\gamma}) = 0. \tag{2}$$

Here, S_f and S_s stand for the fluid and solid Steklov-Poincaré operators which can be defined as follows: for a given interface displacement $\boldsymbol{\gamma}$, $S_f(\boldsymbol{\gamma})$ gives the stress exerted by the fluid on the interface, and analogously for S_s. All these notations will be made precise below. In section 4.2, we shall describe the link between (1) and (2).

Finally, the composition of the inverse operator S_s^{-1} with (2) gives rise to the so-called Dirichlet-to-Neumann formulation:

$$\text{Formulation (III):} \qquad S_s^{-1}\big(-S_f(\boldsymbol{\gamma})\big) - \boldsymbol{\gamma} = 0. \tag{3}$$

Formally speaking, Formulations (II) and (III) are similar. Nevertheless, we prefer to distinguish them since they correspond to different approaches in the literature. The denominations "Dirichlet-Neumann formulation" and "Steklov-Poincaré formulation" are purely conventional (both of them clearly involve Steklov-Poincaré operators).

The three following paragraphs address a brief state-of-the-art on the iterative methods for the numerical solution of (1), (2) and (3).

1.1 Monolithic formulation

A common approach in the numerical solution of nonlinear systems, arising in implicit coupling, consists in applying a Newton based algorithm to the global formulation (1). This requires the repeated solution of a tangent (or approximated tangent) problem with the following block structure:

$$\begin{bmatrix} \mathrm{D}_{\boldsymbol{x}_f}\mathcal{F}(\boldsymbol{x}_f,\boldsymbol{\gamma}) & 0 & \mathrm{D}_{\boldsymbol{\gamma}}\mathcal{F}(\boldsymbol{x}_f,\boldsymbol{\gamma}) \\ 0 & \mathrm{D}_{\boldsymbol{x}_s}\mathcal{S}(\boldsymbol{x}_s,\boldsymbol{\gamma}) & \mathrm{D}_{\boldsymbol{\gamma}}\mathcal{S}(\boldsymbol{x}_s,\boldsymbol{\gamma}) \\ \mathrm{D}_{\boldsymbol{x}_f}\mathcal{I}(\boldsymbol{x}_f,\boldsymbol{x}_s) & \mathrm{D}_{\boldsymbol{x}_s}\mathcal{I}(\boldsymbol{x}_f,\boldsymbol{x}_s) & 0 \end{bmatrix} \begin{bmatrix} \delta\boldsymbol{x}_f \\ \delta\boldsymbol{x}_s \\ \delta\gamma \end{bmatrix} = - \begin{bmatrix} \mathcal{F}(\boldsymbol{x}_f,\boldsymbol{\gamma}) \\ \mathcal{S}(\boldsymbol{x}_s,\boldsymbol{\gamma}) \\ \mathcal{I}(\boldsymbol{x}_f,\boldsymbol{x}_s) \end{bmatrix}. \tag{4}$$

Newton algorithms based on the numerical solution of (4) in a *monolithic* fashion, *i.e.* using global direct or iterative methods, have been reported in [45, 48, 28, 2, 16]. It is worth noticing that such a monolithic approach makes difficult the use of separate solvers for the fluid and structure sub-problems. Alternatively, system (4) can be solved in a *partitioned* manner through a block-Gauss elimination of $\delta\boldsymbol{x}_f$, which leads to the so called block-Newton methods [34, 35, 21, 22].

1.2 Dirichlet to Neumann formulations

Formulation (III) reduces problem (1) to the determination of a fixed point of the *Dirichlet-to-Neumann* operator $\boldsymbol{\gamma} \mapsto S_s^{-1}\big(-S_f(\boldsymbol{\gamma})\big)$. This motivates the use of fixed-point based methods [33, 39, 38, 37]:

$$\boldsymbol{\gamma}^{k+1} = \omega^k S_s^{-1}\big(-S_f(\boldsymbol{\gamma}^k)\big) + (1-\omega^k)\boldsymbol{\gamma}^k, \tag{5}$$

with ω^k a given relaxation parameter which is chosen in order to enhance convergence [38, 37, 13, 31]. Alternatively, one can use Newton based methods [26, 23] for a fast convergence towards the solution of (3). This requires the solution of a tangent problem of the type

$$(J(\boldsymbol{\gamma}^k) - \boldsymbol{I})\delta\gamma = -\big(S_s^{-1}\left(-S_f(\boldsymbol{\gamma}^k)\right) - \boldsymbol{\gamma}^k\big), \tag{6}$$

where $J(\boldsymbol{\gamma})$ stands for the Jacobian, or approximated Jacobian [26], of the composed operator $\boldsymbol{\gamma} \mapsto S_s^{-1}\big(-S_f(\boldsymbol{\gamma})\big)$. It is worth noticing that exact Jacobian computations require shape derivative calculus for the fluid [23] (see also [16, 4]). Let us also stress the fact that these methods are naturally partitioned.

1.3 Symmetric Steklov-Poincaré formulation

The Dirichlet-Neumann formulations share a common feature: their implementation is purely sequential. The Steklov-Poincaré formulation (2) may allow to set up parallel algorithms to solve the interface equation.

Following the presentation of Deparis *et al.* [14], the nonlinear problem (2) can be solved through nonlinear Richardson iterations:

$$P(\boldsymbol{\gamma}^{k+1} - \boldsymbol{\gamma}^k) = \omega^k(-S_f(\boldsymbol{\gamma}^k) - S_s(\boldsymbol{\gamma}^k)), \tag{7}$$

for an appropriate choice of the preconditioner P, namely

$$P_k^{-1} = \alpha^k \left[S_f'(\boldsymbol{\gamma}^k)\right]^{-1} + (1-\alpha^k)\left[S_s'(\boldsymbol{\gamma}^k)\right]^{-1}, \tag{8}$$

where $\boldsymbol{\lambda} \mapsto S_f'(\beta)\cdot\boldsymbol{\lambda}$ is the differential of S_f at β, and $\left[S_f'(\beta)\right]^{-1}$ its inverse. This choice generalizes the standard preconditioners of linear domain decomposition methods (for which $S' = S$). If α_k is $0, 1$ or 0.5 we retrieve, respectively, Dirichlet-Neumann, Neumann-Dirichlet or Neumann-Neumann preconditioners. On the other hand, since equation (2) is nonlinear, one can apply a Newton method,

$$\big(S_f'(\boldsymbol{\gamma}^k) + S_s'(\boldsymbol{\gamma}^k)\big)(\boldsymbol{\gamma}^{k+1} - \boldsymbol{\gamma}^k) = -S_f(\boldsymbol{\gamma}^k) - S_s(\boldsymbol{\gamma}^k), \tag{9}$$

which corresponds to the nonlinear Richardson iteration (7) preconditioned with $P_k = S_f'(\boldsymbol{\gamma}^k) + S_s'(\boldsymbol{\gamma}^k)$ and $\omega^k = 1$. This linear equation can be solved, for example, by an operator-free GMRES algorithm, with or without preconditioning. For instance, in [14] the authors propose to use the preconditioners (8).

The Newton method applied to the Dirichlet-Neumann formulation is not equivalent to the Newton method applied to the Steklov formulation, since the roles played by the fluid and by the structure are not symmetric in the first approach, whereas they are in the second. After linearization, one cannot compose (6) with S_s to retrieve (9). Finally (8) is not equivalent to (9) since in general $(A+B)^{-1} \neq A^{-1} + B^{-1}$.

The advantage of formulation (II) compared to formulation (III) is that the fluid and the structure sub-problems can be solved simultaneously and independently for the residual computation (right-hand sides of (7)) and the application of the preconditioner (S_f' and S_s') as soon as $\alpha \notin \{0, 1\}$. However, as we shall see in section 5.3, a simplified complexity analysis shows that the overall computational costs of both methods might be of the same order, for instance, whenever the cost of the fluid sub-problem solution is cheaper.

The formulations recalled in Sections 1.2 and 1.3 are first based on the coupling conditions, giving rise to a nonlinear equation on the interface, which involves nonlinear sub-problems. The algorithm we introduce in Section 5 first treats the nonlinearity of the whole problem through a Newton method, and uses a Steklov-Poincaré formulation on the tangent problems.

2 Mechanical setting

Let $\widehat{\Omega} = \widehat{\Omega}_f \cup \widehat{\Omega}_s$ be a reference configuration of the system, see Figure 1. We introduce the motion of the solid medium

$$\widehat{\boldsymbol{\varphi}}_s : \widehat{\Omega}_s \times \mathbb{R}^+ \longrightarrow \mathbb{R}^3.$$

The current configuration of the structure is then denoted by

$$\Omega_s(t) = \boldsymbol{\varphi}_s(\widehat{\Omega}_s, t).$$

We introduce the deformation gradient $\widehat{\boldsymbol{F}}_s(\widehat{\boldsymbol{x}}, t) \stackrel{\text{def}}{=} \boldsymbol{\nabla}_{\widehat{\boldsymbol{x}}} \boldsymbol{\varphi}_s(\widehat{\boldsymbol{x}}, t)$, and its determinant $\widehat{J}_s(\widehat{\boldsymbol{x}}, t) \stackrel{\text{def}}{=} \det \widehat{\boldsymbol{F}}_s(\widehat{\boldsymbol{x}}, t)$. The displacement of the solid domain is given by $\widehat{\boldsymbol{d}}_s(\widehat{\boldsymbol{x}}, t) \stackrel{\text{def}}{=} \widehat{\boldsymbol{\varphi}}_s(\widehat{\boldsymbol{x}}, t) - \widehat{\boldsymbol{x}}$. The fluid domain $\Omega_f(t)$ is parametrized by the Arbitrary Lagrangian Eulerian ALE mapping (see [17], for instance),

$$\widehat{\mathcal{A}} : \widehat{\Omega}_f \times \mathbb{R}^+ \longrightarrow \mathbb{R}^3,$$

such that $\Omega_f(t) = \widehat{\mathcal{A}}(\widehat{\Omega}_f, t)$. In the sequel we will use the notation $\widehat{\mathcal{A}}_t \stackrel{\text{def}}{=} \widehat{\mathcal{A}}(\cdot, t)$ and the superscript $\widehat{\ }$ will be related to fields defined on the reference configuration $\widehat{\Omega}_f$ or $\widehat{\Omega}_s$. In addition, for a given Eulerian fluid quantity q (*i.e.* defined in $\Omega_f(t)$ for $t > 0$) we will denote its ALE description by $\widehat{q}$, as a field defined in $\widehat{\Omega}_f \times \mathbb{R}^+$ as

$$\widehat{q}(\widehat{\boldsymbol{x}}, t) = q\big(\widehat{\mathcal{A}}_t(\boldsymbol{x}), t\big), \quad \forall \boldsymbol{x} \in \widehat{\Omega}_f. \tag{10}$$

We introduce the deformation gradient of the fluid domain

$$\widehat{\boldsymbol{F}}_f(\widehat{\boldsymbol{x}}, t) \stackrel{\text{def}}{=} \boldsymbol{\nabla}_{\widehat{x}} \widehat{\mathcal{A}}(\widehat{\boldsymbol{x}}, t),$$

and its determinant $\widehat{J}_f(\widehat{\boldsymbol{x}}, t) \stackrel{\text{def}}{=} \det \widehat{\boldsymbol{F}}_f(\widehat{\boldsymbol{x}}, t)$. The displacement of the fluid domain is given by $\widehat{\boldsymbol{d}}_f(\widehat{\boldsymbol{x}}, t) \stackrel{\text{def}}{=} \widehat{\mathcal{A}}(\widehat{\boldsymbol{x}}, t) - \widehat{\boldsymbol{x}}$ and its velocity by

$$\widehat{\boldsymbol{w}} \stackrel{\text{def}}{=} \frac{\partial \widehat{\mathcal{A}}}{\partial t}.$$

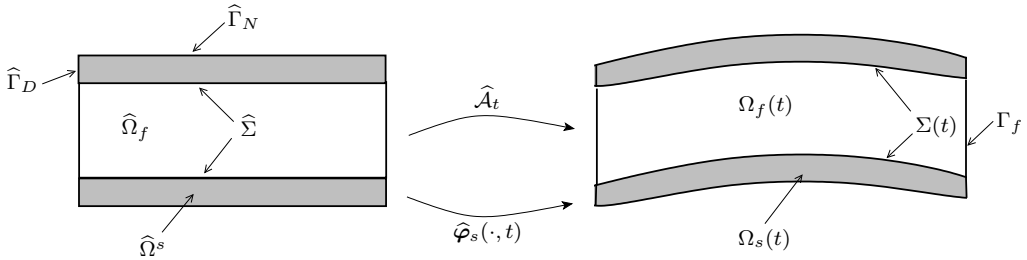

Figure 1: Parametrization of the domains $\Omega_f(t)$ and $\Omega_s(t)$.

The fluid-structure interface, namely $\partial\Omega_f(t) \cap \partial\Omega_s(t)$ is denoted by $\Sigma(t)$, and $\Gamma_f = \partial\Omega_f(t)\backslash\Sigma(t)$ stands for the portion of the fluid boundary that is not shared with the boundary of the structure. The surface Γ_f is assumed to be independent of t. The boundary $\partial\widehat{\Omega}_s$ of the reference configuration for the structure is divided into three disjoint parts $\widehat{\Gamma}_D$, $\widehat{\Gamma}_N$ and $\widehat{\Sigma}$, with $\Sigma(t) = \widehat{\mathcal{A}}_t(\widehat{\Sigma})$. We denote by $\boldsymbol{n}$ the outward unit normal on the fluid boundary in the current configuration, and by $\widehat{\boldsymbol{n}}_s$ the outward unit normal on the reference structure boundary.

2.1 The coupled problem

We consider an homogeneous, Newtonian viscous, incompressible fluid with density ρ_f and dynamic viscosity μ. Its state is described by its Eulerian velocity $\boldsymbol{u}$ and pressure p. The constitutive law for the Cauchy stress tensor is given by the following expression:

$$\boldsymbol{\sigma}(\boldsymbol{u}, p) = -p\boldsymbol{I} + 2\mu\boldsymbol{\epsilon}(\boldsymbol{u}),$$

with $\boldsymbol{\epsilon}(\boldsymbol{u}) \stackrel{\text{def}}{=} \left[\nabla\boldsymbol{u} + (\nabla\boldsymbol{u})^{\mathrm{T}}\right]/2$. In absence of body forces, these unknowns satisfy the incompressible Navier-Stokes equations in an ALE formulation:

$$\left\{\begin{array}{rl} \rho_f \left.\dfrac{\partial \boldsymbol{u}}{\partial t}\right|_{\widehat{\boldsymbol{x}}} + \rho_f(\boldsymbol{u}-\boldsymbol{w})\cdot\boldsymbol{\nabla}\boldsymbol{u} - \operatorname{div}\left(2\mu\boldsymbol{\epsilon}(\boldsymbol{u})\right) + \boldsymbol{\nabla}p = 0, & \text{in} \quad \Omega_f(t), \\ \operatorname{div}\boldsymbol{u} = 0, & \text{in} \quad \Omega_f(t), \\ \boldsymbol{\sigma}(\boldsymbol{u}, p)\cdot\boldsymbol{n} = \boldsymbol{g}, & \text{on} \quad \Gamma_f, \end{array}\right. \tag{11}$$

where $\left.\dfrac{\partial}{\partial t}\right|_{\widehat{\boldsymbol{x}}}$ stands for the ALE time derivative, $\boldsymbol{w} \stackrel{\text{def}}{=} \widehat{\boldsymbol{w}} \circ \widehat{\mathcal{A}}_t^{-1}$, and $\boldsymbol{g}$ a given density of surface force.

The structure is supposed to be hyperelastic under large displacements and deformations. Its density is denoted by ρ_s. Its state is described by its displacement $\widehat{\boldsymbol{d}}_s$ and its first Piola-Kirchoff stress tensor $\widehat{\boldsymbol{T}}$. The latter is related to $\widehat{\boldsymbol{d}}_s$ as the gradient of an internal stored energy function $W(\widehat{\boldsymbol{F}}_s)$. The choice of the internal stored energy will depend on the problem under consideration and will not change the setting of the fluid-structure problem. Assuming that the structure is clamped on Γ_D and under no body and surface forces, these unknowns are driven by the following elastodynamic equations

$$\left\{\begin{array}{rl} \widehat{J}_s\rho_s\dfrac{\partial^2\widehat{\boldsymbol{d}}_s}{\partial t^2} - \operatorname{div}_{\widehat{\boldsymbol{x}}}\widehat{\boldsymbol{T}} = \boldsymbol{0}, & \text{in} \quad \widehat{\Omega}_s, \\ \widehat{\boldsymbol{d}} = \boldsymbol{0}, & \text{on} \quad \widehat{\Gamma}_D, \\ \widehat{\boldsymbol{T}}\cdot\widehat{\boldsymbol{n}}_s = 0, & \text{on} \quad \widehat{\Gamma}_N. \end{array}\right. \tag{12}$$

The coupling between the solid and the fluid, namely equations (11) and (12), is realized through standard boundary conditions at the fluid-structure interface $\Sigma(t)$ that ensure the balance of the mechanical energy over the whole domain. This is achieved by imposing three interface conditions:

- A geometrical condition enforcing the matching between $\boldsymbol{\varphi}_s$ and $\widehat{\mathcal{A}}$ on the interface

$$\widehat{\boldsymbol{d}}_f = \widehat{\boldsymbol{d}}_s, \quad \text{on} \quad \widehat{\Sigma}. \tag{13}$$

Inside $\widehat{\Omega}_f$, the fluid domain displacement $\widehat{\boldsymbol{d}}_f$ can be defined as an arbitrary (suitable) extension of $\widehat{\boldsymbol{d}}_s$ over the domain $\widehat{\Omega}_f$, namely,

$$\widehat{\boldsymbol{d}}_f = \mathrm{Ext}(\widehat{\boldsymbol{d}}_{s|\widehat{\Sigma}}) \tag{14}$$

(see Remark 1 below).

- A kinematic condition enforcing the continuity of the velocities at the interface

$$\boldsymbol{u} = \frac{\partial \widehat{\boldsymbol{d}}_s}{\partial t} \circ \widehat{\mathcal{A}}_t^{-1}, \quad \text{on} \quad \Sigma(t). \tag{15}$$

- And a kinetic condition imposing the stress continuity at the interface

$$\widehat{\boldsymbol{T}}\widehat{\boldsymbol{n}}_s = -\widehat{J}_f \widehat{\boldsymbol{\sigma}(\boldsymbol{u}, p)} \widehat{\boldsymbol{F}}_f^{-T} \widehat{\boldsymbol{n}}, \quad \text{on} \quad \widehat{\Sigma}. \tag{16}$$

To summarize, the fluid-structure system involving an incompressible viscous fluid and a hyperelastic structure is described in terms of the unknowns $(\boldsymbol{u}, p, \widehat{\boldsymbol{d}}_f, \widehat{\boldsymbol{d}}_s)$ satisfying the coupled problem (11)-(16).

Remark 1 *In practice, we can choose as operator Ext a harmonic extension operator, by solving a Laplace equation*

$$\begin{cases} -\mathrm{div}\,(\kappa \boldsymbol{\nabla} \widehat{\boldsymbol{d}}_f) = 0, & on \quad \widehat{\Omega}_f, \\ \widehat{\boldsymbol{d}}_f = \widehat{\boldsymbol{d}}_s, & on \quad \widehat{\Sigma}, \\ \widehat{\boldsymbol{d}}_f = \boldsymbol{0}, & on \quad \widehat{\Gamma}_f, \end{cases} \tag{17}$$

where $\kappa > 0$ is a given "diffusion" coefficient, that can depend on $\widehat{\boldsymbol{d}}_s$. Other alternative extension approaches can be found, for instance, in [3, 46].

Remark 2 *The combination of* (13) *and* (15) *enforces $\boldsymbol{u} = \boldsymbol{w}$ on $\Sigma(t)$. This requirement is not strictly necessary but simplifies the construction of the ALE map. In general we could replace* (14) *by* $\dfrac{\partial \widehat{\boldsymbol{d}}_s}{\partial t} \circ \widehat{\mathcal{A}}_t^{-1} \cdot \boldsymbol{n} = \boldsymbol{w} \cdot \boldsymbol{n}$ *on $\Sigma(t)$.*

Remark 3 *For simplicity, we have only prescribed Neumann boundary conditions in* (11)*. In practice we may use Dirichlet conditions on some part of the boundary.*

2.2 Weak formulation

Problem (11)-(16) can be reformulated in a weak variational form using appropriate test functions, performing integrations by parts and taking into account the boundary and interface conditions.

In what follows, we will make explicit the dependence of $\Omega_f(t)$ and $\Sigma(t)$ on $\widehat{\boldsymbol{d}}_f$ by introducing the notations

$$\Omega_f(\widehat{\boldsymbol{d}}_f) \stackrel{\text{def}}{=} \Omega_f(t), \quad \Sigma(\widehat{\boldsymbol{d}}_f) \stackrel{\text{def}}{=} \Sigma(t).$$

Let $(\widehat{\boldsymbol{v}_f}, \widehat{q}) \in [H^1(\widehat{\Omega}_f)]^3 \times L^2(\widehat{\Omega}_f)$, multiplying the fluid problem (11) by $(\boldsymbol{v}_f, q) = (\widehat{\boldsymbol{v}_f} \circ \widehat{\mathcal{A}}_t^{-1}, \widehat{q} \circ \widehat{\mathcal{A}}_t^{-1})$ integrating over $\Omega_f(\widehat{\boldsymbol{d}_f})$ and after integrations by parts we get

$$\begin{aligned}\frac{\mathrm{d}}{\mathrm{dt}} \int_{\Omega_f(\widehat{\boldsymbol{d}_f})} \rho_f \boldsymbol{u} \cdot \boldsymbol{v}_f \,\mathrm{d}\boldsymbol{x} + \int_{\Omega_f(\widehat{\boldsymbol{d}_f})} \mathrm{div}\left[\rho_f \boldsymbol{u} \otimes \left(\boldsymbol{u} - \boldsymbol{w}(\widehat{\boldsymbol{d}_f})\right)\right] \cdot \boldsymbol{v}_f \,\mathrm{d}\boldsymbol{x} \\ + \int_{\Omega_f(\widehat{\boldsymbol{d}_f})} \boldsymbol{\sigma}(\boldsymbol{u}, p) : \nabla \boldsymbol{v}_f \,\mathrm{d}\boldsymbol{x} - \int_{\Sigma(\widehat{\boldsymbol{d}_f})} \boldsymbol{\sigma}(\boldsymbol{u}, p) \cdot \boldsymbol{v}_f \cdot \boldsymbol{n} \\ \mathrm{d}\boldsymbol{a} - \int_{\Gamma_{\mathrm{in-out}}} \boldsymbol{g} \cdot \boldsymbol{v}_f \,\mathrm{d}\boldsymbol{a} - \int_{\Omega_f(\widehat{\boldsymbol{d}_f})} q \,\mathrm{div}\, \boldsymbol{u} \,\mathrm{d}\boldsymbol{x} = 0,\end{aligned}$$

where

$$\boldsymbol{w}(\widehat{\boldsymbol{d}_f}) = \frac{\partial \widehat{\boldsymbol{d}_f}}{\partial t} \circ \widehat{\mathcal{A}}_t^{-1}.$$

For the structure, multiplying (12) by $\widehat{\boldsymbol{v}_s} \in [H^1_{\Gamma_D}(\widehat{\Omega}_s)]^3$, integrating by parts over $\widehat{\Omega}_s$, one gets

$$\int_{\widehat{\Omega}_s} \rho_0 \frac{\partial^2 \widehat{\boldsymbol{d}_s}}{\partial t^2} \cdot \widehat{\boldsymbol{v}_s} \,\mathrm{d}\hat{\boldsymbol{x}} + \int_{\widehat{\Omega}_s} \frac{\partial W}{\partial F}(\mathrm{I} + \nabla \widehat{\boldsymbol{d}_s}) : \nabla \widehat{\boldsymbol{v}_s} \,\mathrm{d}\hat{\boldsymbol{x}} - \int_{\widehat{\Sigma}} \frac{\partial W}{\partial F}(\mathrm{I} + \nabla \widehat{\boldsymbol{d}_s}) \widehat{\boldsymbol{n}}_s \cdot \widehat{\boldsymbol{v}_s} \,\mathrm{d}\hat{\boldsymbol{a}} = 0,$$

where $\rho_0 = \widehat{J}_s \rho_s$. Therefore, taking into account the coupling condition (16), it follows that

$$\begin{aligned}\frac{\mathrm{d}}{\mathrm{dt}} \int_{\Omega_f(\widehat{\boldsymbol{d}_f})} \rho_f \boldsymbol{u} \cdot \boldsymbol{v}_f \,\mathrm{d}\boldsymbol{x} + \int_{\Omega_f(\widehat{\boldsymbol{d}_f})} \mathrm{div}\left[\rho_f \boldsymbol{u} \otimes \left(\boldsymbol{u} - \boldsymbol{w}(\widehat{\boldsymbol{d}_f})\right)\right] \cdot \boldsymbol{v}_f \,\mathrm{d}\boldsymbol{x} \\ + \int_{\Omega_f(\widehat{\boldsymbol{d}_f})} \boldsymbol{\sigma}(\boldsymbol{u}, p) : \nabla \boldsymbol{v}_f \,\mathrm{d}\boldsymbol{x} - \int_{\Gamma_{\mathrm{in-out}}} \boldsymbol{g} \cdot \boldsymbol{v}_f \,\mathrm{d}\boldsymbol{a} - \int_{\Omega_f(\widehat{\boldsymbol{d}_f})} q \,\mathrm{div}\, \boldsymbol{u} \,\mathrm{d}\boldsymbol{x} \\ + \int_{\widehat{\Omega}_s} \rho_0 \frac{\partial^2 \widehat{\boldsymbol{d}_s}}{\partial t^2} \cdot \widehat{\boldsymbol{v}_s} \,\mathrm{d}\hat{\boldsymbol{x}} + \int_{\widehat{\Omega}_s} \frac{\partial W}{\partial F}(\mathrm{I} + \nabla \widehat{\boldsymbol{d}_s}) : \nabla \widehat{\boldsymbol{v}_s} \,\mathrm{d}\hat{\boldsymbol{x}} = 0, \quad (18)\end{aligned}$$

for all $(\widehat{\boldsymbol{v}_f}, \widehat{q}) \in [H^1(\widehat{\Omega}_f)]^3 \times L^2(\widehat{\Omega}_f)$ and $\widehat{\boldsymbol{v}_s} \in [H^1_{\Gamma_D}(\widehat{\Omega}_s)]^3$ with $\widehat{\boldsymbol{v}_f} = \widehat{\boldsymbol{v}_s}$ on $\widehat{\Sigma}$. The weak form of the geometry coupling conditions (13) and (14) are rewritten in terms of the interface displacement $\boldsymbol{\gamma} \in [H^{\frac{1}{2}}(\widehat{\Sigma})]^3$ as

$$\int_{\widehat{\Omega}_f} \left(\widehat{\boldsymbol{d}_f} - \mathrm{Ext}(\boldsymbol{\gamma})\right) \cdot \widehat{\boldsymbol{\tau}} \,\mathrm{d}\hat{\boldsymbol{x}} + \int_{\widehat{\Sigma}} (\widehat{\boldsymbol{d}_s} - \boldsymbol{\gamma}) \cdot \widehat{\boldsymbol{\zeta}} \,\mathrm{d}\hat{\boldsymbol{a}} = 0, \quad (19)$$

for all $\widehat{\boldsymbol{\tau}} \in [L^2(\widehat{\Omega}_f)]^3$ and $\widehat{\boldsymbol{\zeta}} \in [L^2(\widehat{\Sigma})]^3$. Finally, the continuity of the velocities at the interface (15) is reformulated as

$$\int_{\widehat{\Sigma}} \left(\widehat{\boldsymbol{u}} - \widehat{\boldsymbol{w}}(\widehat{\boldsymbol{d}_f})\right) \cdot \widehat{\boldsymbol{\xi}} \,\mathrm{d}\hat{\boldsymbol{a}} = 0, \quad (20)$$

for all $\widehat{\boldsymbol{\xi}} \in [L^2(\widehat{\Sigma})]^3$.

Therefore, after summation of (18)-(20) we obtain the following global weak formulation of problem (11)-(16): Find $\widehat{\boldsymbol{u}} : \widehat{\Omega}_f \times \mathbb{R}^+ \to \mathbb{R}^3$, $\widehat{p} : \widehat{\Omega}_f \times \mathbb{R}^+ \to \mathbb{R}$,

$\widehat{\boldsymbol{d}}_f : \widehat{\Omega}_f \times \mathbb{R}^+ \to \mathbb{R}^3$, $\widehat{\boldsymbol{d}}_s : \widehat{\Omega}_s \times \mathbb{R}^+ \to \mathbb{R}^3$ and $\boldsymbol{\gamma} : \widehat{\Sigma} \times \mathbb{R}^+ \to \mathbb{R}^3$ such that

$$\begin{aligned}
&\frac{\mathrm{d}}{\mathrm{dt}} \int_{\Omega_f(\widehat{\boldsymbol{d}_f})} \rho_f \boldsymbol{u} \cdot \boldsymbol{v}_f \,\mathrm{d}\boldsymbol{x} + \int_{\Omega_f(\widehat{\boldsymbol{d}_f})} \mathrm{div}\left[\rho_f \boldsymbol{u} \otimes \left(\boldsymbol{u} - \boldsymbol{w}\big(\widehat{\boldsymbol{d}_f}\big)\right)\right] \cdot \boldsymbol{v}_f \,\mathrm{d}\boldsymbol{x} \\
&\qquad + \int_{\Omega_f(\widehat{\boldsymbol{d}_f})} \boldsymbol{\sigma}(\boldsymbol{u}, p) : \nabla \boldsymbol{v}_f \,\mathrm{d}\boldsymbol{x} - \int_{\Gamma_{\mathrm{in-out}}} \boldsymbol{g} \cdot \boldsymbol{v}_f \,\mathrm{d}\boldsymbol{a} - \int_{\Omega_f(\widehat{\boldsymbol{d}_f})} q \,\mathrm{div}\, \boldsymbol{u} \,\mathrm{d}\boldsymbol{x} \\
&+ \int_{\widehat{\Omega}_s} \rho_0 \frac{\partial^2 \widehat{\boldsymbol{d}_s}}{\partial t^2} \cdot \widehat{\boldsymbol{v}_s} \,\mathrm{d}\hat{\boldsymbol{x}} + \int_{\widehat{\Omega}_s} \frac{\partial W}{\partial F}(\mathrm{I} + \nabla \widehat{\boldsymbol{d}_s}) : \nabla \widehat{\boldsymbol{v}_s} \,\mathrm{d}\hat{\boldsymbol{x}} + \int_{\widehat{\Omega}_f} \left(\widehat{\boldsymbol{d}_f} - \mathrm{Ext}(\boldsymbol{\gamma})\right) \cdot \widehat{\boldsymbol{\tau}} \,\mathrm{d}\hat{\boldsymbol{x}} \\
&\qquad + \int_{\widehat{\Sigma}} (\widehat{\boldsymbol{d}_s} - \boldsymbol{\gamma}) \cdot \widehat{\boldsymbol{\zeta}} \,\mathrm{d}\hat{\boldsymbol{a}} + \int_{\widehat{\Sigma}} \left(\widehat{\boldsymbol{u}} - \widehat{\boldsymbol{w}}(\widehat{\boldsymbol{d}_f})\right) \cdot \widehat{\boldsymbol{\xi}} \,\mathrm{d}\hat{\boldsymbol{a}} = 0, \quad (21)
\end{aligned}$$

with $\boldsymbol{u}(\cdot, t) = \widehat{\boldsymbol{u}}(\cdot, t) \circ \widehat{\mathcal{A}}_t^{-1}$, $p(\cdot, t) = \widehat{p}(\cdot, t) \circ \widehat{\mathcal{A}}_t^{-1}$, and for all $(\widehat{\boldsymbol{v}_f}, \widehat{q}) \in [H^1(\widehat{\Omega}_f)]^3 \times L^2(\widehat{\Omega}_f)$, $\boldsymbol{v}_s \in [H^1_{\Gamma_D}(\widehat{\Omega}_s)]^3$ with $\widehat{\boldsymbol{v}_f} = \widehat{\boldsymbol{v}_s}$ on $\widehat{\Sigma}$, $\widehat{\boldsymbol{\tau}} \in [L^2(\widehat{\Omega}_f)]^3$, $\widehat{\boldsymbol{\zeta}} \in [L^2(\widehat{\Sigma})]^3$ and $\widehat{\boldsymbol{\xi}} \in [L^2(\widehat{\Sigma})]^3$.

3 Constitutive laws for artery walls

3.1 Three dimensional constitutive laws

In an extensive survey article [29], Holzapfel *et al.* have analyzed and compared existing constitutive models for arterial walls. They have also introduced a new framework to take into account anisotropy and various mechanical effects such as inflation and torsion. Their model is based on a thick-walled nonlinearly elastic tube consisting of two layers. Another model has been introduced by van Oijen in his PhD thesis [40]. More microscopically based, it uses the mixing theory to take into account the fibers in the layers. Even more precise at the microscopic level, Caillerie *et al.* have introduced a nonlinear homogenization approach to fiber-reinforcement in soft tissues ([7]).

These three models have two common features: they are three-dimensional and anisotropic. Previous approaches, such as the Fung model in [25], are based on geometrical simplifications, such as membrane, and more generally on thin shell. However, as pointed out in [29], such simplifications are not suitable for the analysis of the through-thickness stress distribution in an artery or for the treatment of shearing deformations. In addition, the combination of inflation and torsion effects cannot be reproduced by such simplified models. This may explain why three-dimensional constitutive laws are needed to correctly handle the passive mechanical behavior of artery walls.

From a physiological point of view, the arterial wall is made of three layers (the intima, the media and the adventitia). For a healthy artery, only the media and the adventitia have a significant mechanical role. In addition, their mechanical behavior is highly anisotropic due to the presence of fibers (collagenous components). In [29], Holzapfel *et al.* propose a model based on two layers modeling the media and the adventitia. For both layers, the material is supposed to be three-dimensional, thin, hyperelastic, in finite deformation, incompressible, anisotropic (in the fiber directions) and pre-stressed.

The elastic assumption is well satisfied in some vessels, as the aorta, the iliac and carotid arteries. For other arteries, including the femoral, celiac and cerebral arteries, viscoelastic models are needed.

As a consequence of the above assumptions, the free energy of a layer can be written as

$$W(\widehat{\boldsymbol{F}}_s) = \Psi_{\rm iso}(I_1, I_2, J) + \Psi_{\rm fib}(I_4, I_5), \tag{22}$$

where $\widehat{\boldsymbol{F}}_s$ is the deformation gradient, I_1, I_2 and J its three principal invariants and I_4 and I_5 its pseudo-invariants related to the reinforcement direction. The first part of the energy $\Psi_{\rm iso}$ is isotropic, typically a neo-Hookean, Mooney-Rivlin or Ciarlet-Geymonat type of energy. The second part $\Psi_{\rm fib}$ is anisotropic and involves an exponential term in order to reproduce the strong stiffening effect of each layer at high pressure.

From a computational point of view, the above combination of mechanical properties gives rise to two major difficulties: the treatment of incompressibility in finite deformation and the treatment of bad aspect ratios for thin three-dimensional structures. Both phenomena lead to locking problems ([9],[12]) if not correctly treated. Incompressibility issues are classically dealt with using a mixed finite element method, whereas locking phenomena in thin three-dimensional structures are treated using re-interpolation techniques [10, 12, 11] as presented in the following subsection.

3.2 3D shell elements

A general structural model of the blood flow with complex and realistic geometries has to be three-dimensional and handle large displacements.

Since the wall of the blood vessels is thin, it is convenient to use shell elements; they accurately describe its geometry. All finite elements adopted in our simulations are general shell elements. Previously, Gerbeau *et al.* have used the MITC4 elements [26, 27] with a 3D constitutive law for which the transversal stress is null and a kinematic constraint is needed to make the model compatible with a Reissner-Mindlin shell model. This restricts the choice of the energy.

We consider here 3D-shell elements [10, 12, 11]. These elements appear as standard three-dimensional elements. Thus it is very easy to couple them to other three-dimensional formulations through the nodes on the faces. The element considered here, called MI3D, uses standard 3D $\mathbb{Q}_2$ shape functions. The advantage of a quadratic approximation in the shell's thickness is that it is possible to deal with standard 3D energies, such as generalized Hook or any hyperelastic stored energy, defined by using the Cauchy-Green tensor's invariants, such as the one defined in (22).

In order to be able to apply MITC techniques to stabilize the formulation, it is necessary to compute the first and second derivatives of the stored energy with respect to the Green-Lagrange tensor, defined hereafter, in local coordinates (r, s, z), as it is usually done in shell element (see Figure 2):

$$e_{ij}(\vec{U}) \stackrel{\rm def}{=} \frac{1}{2}(\vec{g}_i \cdot \vec{U}_{,j} + \vec{g}_j \cdot \vec{U}_{,i} + \vec{U}_{,i} \cdot \vec{U}_{,j}), \tag{23}$$

where $\vec{g}_i$ is a covariant basis.

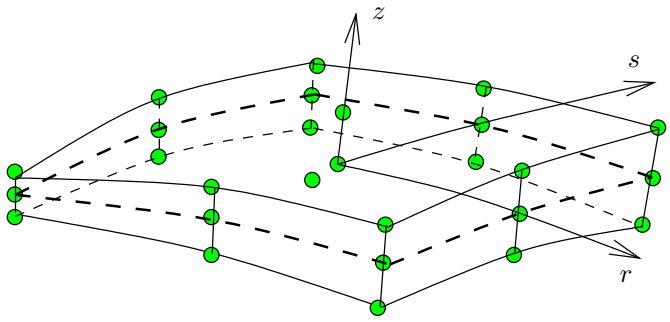

Figure 2: 3D shell element

The first and second order infinitesimal variations are given by

$$\delta e_{ij} = \frac{1}{2}(\vec{g}_i \cdot \delta\vec{U}_{,j} + \vec{g}_j \cdot \delta\vec{U}_{,i} + \vec{U}_{,i} \cdot \delta\vec{U}_{,j} + \vec{U}_{,j} \cdot \delta\vec{U}_{,i}),$$
$$d\delta e_{ij} = \frac{1}{2}(d\vec{U}_{,i} \cdot \delta\vec{U}_{,j} + d\vec{U}_{,j} \cdot \delta\vec{U}_{,i}).$$

At each time level of the Newmark time-discretization, a nonlinear problem has to be solved. The bilinear form appearing in this algorithm is the following:

$$A = A^L + A^{NL},$$

with

$$A^L(d\vec{U}, \delta\vec{U}) \stackrel{\text{def}}{=} \int_\Omega \frac{\partial^2 W}{\partial e_{ij}\partial e_{kl}} de_{kl}\delta e_{ij}\, dV, \tag{24}$$

$$A^{NL}(d\vec{U}, \delta\vec{U}) \stackrel{\text{def}}{=} \int_\Omega \frac{\partial W}{\partial e_{ij}} d\delta e_{ij}\, dV, \tag{25}$$

and the corresponding nonlinear right-hand side

$$F^{NL}(\delta\vec{U}) \stackrel{\text{def}}{=} \int_\Omega \frac{\partial W}{\partial e_{ij}} \delta e_{ij}\, dV. \tag{26}$$

In practice, the values of the deformation are not directly computed by (23), but are re-interpolated at the tying points defined by MITC methods. The first and second order infinitesimal variations in (24)–(26) have to be re-interpolated using the same rules in order to obtain a consistent tangent problem.

Both the MITC4 and the MI3D elements can be employed in actual computations. The MITC4 with 4 nodes and 5 degrees of freedom per node has 20 degrees of freedom per element, the MI3D with 27 nodes and 3 degrees of freedom per node has 81 degrees of freedom per element. The MI3D is indeed more expensive than the MITC4 but it is more convenient for realistic models of the arteries, as recalled at the beginning of this section.

In Section 6, we present some numerical tests using MI3D elements with a neo-Hookean constitutive law in finite deformation, thus tackling the two major numerical difficulties for the implementation of the thick-walled nonlinearly elastic bilayer constitutive laws introduced in [29]. This example provides us with a case of interest for which the numerical method developed in Section 5 may be competitive.

4 Semi-discretized weak formulation

In this section, the weak coupled formulation (21) is semi-discretized in time using an implicit coupling-scheme. The resulting nonlinear problem will be turned into an abstract form. This will allow us to introduce in the next section general nonlinear iterative solution methods.

4.1 Implicit coupling scheme

We use an implicit Euler scheme for the ALE Navier-Stokes equations, with a semi-implicit treatment of the nonlinear convective term. Furthermore we use a mid-point rule for the structural equation. Thus, given a time step $\delta t > 0$, for $n = 0, 1, \ldots$, the time semi-discretized coupled problem writes: Given $\left(\widehat{\boldsymbol{u}}^n, \widehat{p}^n, \widehat{\boldsymbol{d}_f}^n, \widehat{\boldsymbol{d}_s}^n, \boldsymbol{\gamma}^n\right)$, find

$$\left(\widehat{\boldsymbol{u}}^{n+1}, \widehat{p}^{n+1}, \widehat{\boldsymbol{d}_f}^{n+1}, \widehat{\boldsymbol{d}_s}^{n+1}, \boldsymbol{\gamma}^{n+1}\right) \in [H^1(\widehat{\Omega}_f)]^3 \times L^2(\widehat{\Omega}_f) \times [H^1(\widehat{\Omega}_f)]^3 \times [H^1(\widehat{\Omega}_s)]^3 \times [H^{\frac{1}{2}}(\widehat{\Sigma})]^3,$$

such that

$$\begin{aligned}
&\frac{1}{\delta t}\int_{\Omega_f(\widehat{\boldsymbol{d}}_f^{n+1})} \rho_f \boldsymbol{u}^{n+1}\cdot\boldsymbol{v}_f \,\mathrm{d}\boldsymbol{x} - \frac{1}{\delta t}\int_{\Omega_f(\widehat{\boldsymbol{d}}_f^{n})} \rho_f \boldsymbol{u}^{n}\cdot\boldsymbol{v}_f \,\mathrm{d}\boldsymbol{x} \\
&\qquad + \int_{\Omega_f(\widehat{\boldsymbol{d}}_f^{n+1})} \boldsymbol{\sigma}(\boldsymbol{u}^{n+1}, p^{n+1}) : \nabla \boldsymbol{v}_f \,\mathrm{d}\boldsymbol{x} \\
&\qquad + \int_{\Omega_f(\widehat{\boldsymbol{d}}_f^{n+1})} \mathrm{div}\left[\rho_f \boldsymbol{u}^{n+1} \otimes \left(\boldsymbol{u}^n - \boldsymbol{w}\left(\widehat{\boldsymbol{d}_f}^{n+1}\right)\right)\right]\cdot \boldsymbol{v}_f \,\mathrm{d}\boldsymbol{x} \\
&- \int_{\Gamma_{\mathrm{in-out}}} \boldsymbol{g}^{n+1}\cdot\boldsymbol{v}_f \,\mathrm{d}\boldsymbol{a} - \int_{\Omega_f(\widehat{\boldsymbol{d}}_f^{n+1})} q\,\mathrm{div}\,\boldsymbol{u}^{n+1}\,\mathrm{d}\boldsymbol{x} + \int_{\widehat{\Omega}_f}\left(\widehat{\boldsymbol{d}}_f^{n+1} - \mathrm{Ext}\left(\boldsymbol{\gamma}^{n+1}\right)\right)\cdot\widehat{\boldsymbol{\tau}}\,\mathrm{d}\hat{\boldsymbol{x}} \\
&\qquad + \int_{\widehat{\Sigma}}\left(\widehat{\boldsymbol{u}}^{n+1} - \widehat{\boldsymbol{w}}\left(\widehat{\boldsymbol{d}}_f^{n+1}\right)\right)\cdot\widehat{\boldsymbol{\xi}}\,\mathrm{d}\hat{\boldsymbol{a}} + \frac{2}{\delta t^2}\int_{\widehat{\Omega}_s}\rho_0\widehat{\boldsymbol{d}}_s^{n+1}\cdot\widehat{\boldsymbol{v}}_s\,\mathrm{d}\hat{\boldsymbol{x}} \\
&- \frac{2}{\delta t^2}\int_{\widehat{\Omega}_s}\rho_0\left(\widehat{\boldsymbol{d}}_s^n + \Delta t\dot{\widehat{\boldsymbol{d}}}_s^n\right)\cdot\widehat{\boldsymbol{v}}_s\,\mathrm{d}\hat{\boldsymbol{x}} + \int_{\widehat{\Omega}_s}\frac{\partial W}{\partial F}\left(I + \frac{1}{2}\nabla(\widehat{\boldsymbol{d}}_s^n + \widehat{\boldsymbol{d}}_s^{n+1})\right) : \nabla\widehat{\boldsymbol{v}}_s\,\mathrm{d}\hat{\boldsymbol{x}} \\
&\qquad + \int_{\widehat{\Sigma}}\left(\widehat{\boldsymbol{d}}_s^{n+1} - \boldsymbol{\gamma}^{n+1}\right)\cdot\widehat{\boldsymbol{\zeta}}\,\mathrm{d}\hat{\boldsymbol{a}} = 0, \quad (27)
\end{aligned}$$

for all $(\widehat{\boldsymbol{v}_f}, \widehat{q}, \widehat{\boldsymbol{\xi}}, \widehat{\boldsymbol{\tau}}, \widehat{\boldsymbol{\zeta}}, \widehat{\boldsymbol{v}}_s) \in [H^1(\widehat{\Omega}_f)]^3 \times L^2(\widehat{\Omega}_f) \times [L^2(\widehat{\Sigma})]^3 \times [L^2(\widehat{\Omega}_f)]^3 \times [L^2(\widehat{\Sigma})]^3 \times [H^1_{\Gamma_D}(\widehat{\Omega}_s)]^3$ such that $\widehat{\boldsymbol{v}_f} = \widehat{\boldsymbol{v}}_s$ on $\widehat{\Sigma}$, and with $\boldsymbol{u}^n = \widehat{\boldsymbol{u}}^n \circ (\boldsymbol{I} + \widehat{\boldsymbol{d}_f}^n)^{-1}$ (analogously for p^n) and $\dot{\widehat{\boldsymbol{d}}}_s^{n+1} = \frac{2}{\delta t}\left(\widehat{\boldsymbol{d}}_s^{n+1} - \widehat{\boldsymbol{d}}_s^n\right) - \dot{\widehat{\boldsymbol{d}}}_s^n$.

4.2 Abstract formulations

Problem (27) can be rewritten in a more compact form in terms of the fluid, solid and interface state operators. This is the aim of the following paragraphs.

Based on the discrete weak formulation (27) we introduce the fluid operator

$$\mathcal{F} : [H^1(\widehat{\Omega}_f)]^3 \times L^2(\widehat{\Omega}_f) \times [H^1(\widehat{\Omega}_f)]^3 \times [H^{\frac{1}{2}}(\widehat{\Sigma})]^3 \longrightarrow \left([H^1_{\widehat{\Sigma}}(\widehat{\Omega}_f)]^3 \times L^2(\widehat{\Omega}_f) \times [L^2(\widehat{\Sigma})]^3 \times [L^2(\widehat{\Omega}_f)]^3\right)',$$

defined by

$$\begin{aligned}
\left\langle \mathcal{F}\left(\widehat{\boldsymbol{u}}, \widehat{p}, \widehat{\boldsymbol{d}}_f, \boldsymbol{\gamma}\right), \left(\widehat{\boldsymbol{v}_f}, \widehat{q}, \widehat{\boldsymbol{\xi}}, \widehat{\boldsymbol{\tau}}\right)\right\rangle &= \frac{1}{\Delta t}\int_{\Omega_f(\widehat{\boldsymbol{d}}_f)} \rho_f \boldsymbol{u}\cdot\boldsymbol{v}_f \,\mathrm{d}\boldsymbol{x} \\
&- \frac{1}{\Delta t}\int_{\Omega_f(\widehat{\boldsymbol{d}}_f^n)} \rho_f \boldsymbol{u}^n\cdot\boldsymbol{v}_f \,\mathrm{d}\boldsymbol{x} \\
&+ \int_{\Omega_f(\widehat{\boldsymbol{d}}_f)} \mathrm{div}\left[\rho_f \boldsymbol{u}\otimes\left(\boldsymbol{u}^n - \boldsymbol{w}\left(\widehat{\boldsymbol{d}}_f\right)\right)\right]\cdot\boldsymbol{v}_f \,\mathrm{d}\boldsymbol{x} \\
&+ \int_{\Omega_F(\widehat{\boldsymbol{d}}_f)} \boldsymbol{\sigma}(\boldsymbol{u},p) : \nabla\boldsymbol{v}_f \,\mathrm{d}\boldsymbol{x} - \int_{\Gamma_{\mathrm{in-out}}(\widehat{\boldsymbol{d}}_f)} \boldsymbol{g}^{n+1}\cdot\boldsymbol{v}_f \,\mathrm{d}\boldsymbol{a} \\
&- \int_{\Omega_f(\widehat{\boldsymbol{d}}_f)} q\,\mathrm{div}\,\boldsymbol{u} \,\mathrm{d}\boldsymbol{x} + \int_{\widehat{\Sigma}} \left(\widehat{\boldsymbol{u}} - \widehat{\boldsymbol{w}}\left(\widehat{\boldsymbol{d}}_f\right)\right)\cdot\widehat{\boldsymbol{\xi}} \,\mathrm{d}\hat{\boldsymbol{a}} \\
&+ \int_{\widehat{\Omega}_f} \left(\widehat{\boldsymbol{d}}_f - \mathrm{Ext}(\boldsymbol{\gamma})\right)\cdot\widehat{\boldsymbol{\tau}} \,\mathrm{d}\hat{\boldsymbol{x}},
\end{aligned} \tag{28}$$

for all $(\widehat{\boldsymbol{v}_f}, \widehat{q}, \widehat{\boldsymbol{\xi}}, \widehat{\boldsymbol{\tau}}) \in [H^1(\widehat{\Omega}_f)]^3 \times L^2(\widehat{\Omega}_f) \times [L^2(\widehat{\Sigma})]^3 \times [L^2(\widehat{\Omega}_f)]^3$.

Analogously, from (27), the solid operator

$$\mathcal{S} : [H^1(\widehat{\Omega}_s)]^3 \times [H^{\frac{1}{2}}(\widehat{\Sigma})]^3 \longrightarrow ([H^1_{\Gamma_D\cup\widehat{\Sigma}}(\widehat{\Omega}_s)]^3 \times [L^2(\widehat{\Sigma})]^3)',$$

is given by

$$\begin{aligned}
\left\langle \mathcal{S}(\widehat{\boldsymbol{d}}_s, \boldsymbol{\gamma}), (\widehat{\boldsymbol{v}}_s, \widehat{\boldsymbol{\zeta}})\right\rangle &= \frac{2}{\delta t^2}\int_{\widehat{\Omega}_s} \rho_0 \widehat{\boldsymbol{d}}_s\cdot\boldsymbol{v}_s \,\mathrm{d}\hat{\boldsymbol{x}} - \frac{2}{\delta t^2}\int_{\widehat{\Omega}_s} \rho_0\left(\widehat{\boldsymbol{d}}_s^n + \delta t\dot{\widehat{\boldsymbol{d}}}_s^n\right)\cdot\boldsymbol{v}_s \,\mathrm{d}\hat{\boldsymbol{x}} \\
&+ \int_{\widehat{\Omega}_s} \frac{\partial W}{\partial F}\left(I + \frac{1}{2}\nabla\left(\widehat{\boldsymbol{d}}_s^n + \widehat{\boldsymbol{d}}_s\right)\right) : \nabla\widehat{\boldsymbol{v}}_s \,\mathrm{d}\hat{\boldsymbol{x}} + \int_{\widehat{\Sigma}} (\widehat{\boldsymbol{d}}_s - \boldsymbol{\gamma})\cdot\widehat{\boldsymbol{\zeta}} \,\mathrm{d}\hat{\boldsymbol{a}},
\end{aligned} \tag{29}$$

for all $(\widehat{\boldsymbol{v}}_s, \widehat{\boldsymbol{\zeta}}) \in [H^1_{\Gamma_D}(\widehat{\Omega}_s)]^3 \times [L^2(\widehat{\Sigma})]^3$.

Finally, let

$$\mathcal{L}_f : [H^{\frac{1}{2}}(\widehat{\Sigma})]^3 \to [H^1_{\Gamma_{\mathrm{in-out}}}(\widehat{\Omega}_f)]^3$$

and

$$\mathcal{L}_s : [H^{\frac{1}{2}}(\widehat{\Sigma})]^3 \to [H^1_{\partial\widehat{\Omega}_s\setminus\widehat{\Sigma}}(\widehat{\Omega}_s)]^3$$

be two given continuous linear lift operators. The interface operator

$$\mathcal{I} : [H^1(\widehat{\Omega}_f)]^3 \times L^2(\widehat{\Omega}_f) \times [H^1(\widehat{\Omega}_f)]^3 \times [H^1(\widehat{\Omega}_s)]^3 \longrightarrow [H^{-\frac{1}{2}}(\widehat{\Sigma})]^3,$$

is then defined by

$$\left\langle \mathcal{I}\left(\widehat{\boldsymbol{u}}, \widehat{p}, \widehat{\boldsymbol{d}}_f, \widehat{\boldsymbol{d}}_s\right), \boldsymbol{\mu}\right\rangle = \left\langle \mathcal{F}(\widehat{\boldsymbol{u}}, \widehat{p}, \widehat{\boldsymbol{d}}_f, \boldsymbol{\gamma}), (\mathcal{L}_f\boldsymbol{\mu}, 0, \mathbf{0}, \mathbf{0})\right\rangle + \left\langle \mathcal{S}(\widehat{\boldsymbol{d}}_s, \boldsymbol{\gamma}), (\mathcal{L}_s\boldsymbol{\mu}, \mathbf{0})\right\rangle, \tag{30}$$

for all $\boldsymbol{\mu} \in [H^{\frac{1}{2}}(\widehat{\Sigma})]^3$.

Remark 4 *The interface operator does not depend on* $\boldsymbol{\gamma}$ *since, due to the choice of the test functions, the terms involving* $\boldsymbol{\gamma}$ *vanish in the right-hand side of* (30).

According to the above definitions, problem (27) is equivalent to

$$\text{Formulation (I):} \qquad \begin{cases} \mathcal{F}\left(\widehat{\boldsymbol{u}}^{n+1}, \widehat{p}^{n+1}, \widehat{\boldsymbol{d}}_f^{n+1}, \boldsymbol{\gamma}^{n+1}\right) = 0, \\ \mathcal{S}\left(\widehat{\boldsymbol{d}}_s^{n+1}, \boldsymbol{\gamma}^{n+1}\right) = 0, \\ \mathcal{I}\left(\widehat{\boldsymbol{u}}^{n+1}, \widehat{p}^{n+1}, \widehat{\boldsymbol{d}}_f^{n+1}, \widehat{\boldsymbol{d}}_s^{n+1}\right) = 0. \end{cases} \tag{31}$$

4.3 Steklov-Poincaré operators

In order to describe partitioned methods for the numerical solution of (27), we now introduce the nonlinear fluid and solid Steklov-Poincaré operators.

The nonlinear fluid Steklov-Poincaré operator

$$S_f : [H^{\frac{1}{2}}(\widehat{\Sigma})]^3 \longrightarrow [H^{-\frac{1}{2}}(\widehat{\Sigma})]^3,$$

is defined by

$$\langle S_f(\boldsymbol{\gamma}), \boldsymbol{\mu} \rangle = \left\langle \mathcal{I}\big(\widehat{\boldsymbol{u}}(\boldsymbol{\gamma}), \widehat{p}(\boldsymbol{\gamma}), \widehat{\boldsymbol{d}}_f(\boldsymbol{\gamma}), \mathbf{0}\big), \boldsymbol{\mu} \right\rangle,$$

for all $\boldsymbol{\gamma}, \boldsymbol{\mu} \in [H^{\frac{1}{2}}(\hat{\Sigma})]^3$, where $\big(\widehat{\boldsymbol{u}}(\boldsymbol{\gamma}), \widehat{p}(\boldsymbol{\gamma}), \widehat{\boldsymbol{d}}_f(\boldsymbol{\gamma})\big)$ is the solution of the Dirichlet fluid problem:

$$\mathcal{F}\left(\widehat{\boldsymbol{u}}(\boldsymbol{\gamma}), \widehat{p}(\boldsymbol{\gamma}), \widehat{\boldsymbol{d}_f}(\boldsymbol{\gamma}), \boldsymbol{\gamma}\right) = 0.$$

In an analogous way, we introduce the nonlinear solid Steklov-Poincaré operator

$$S_s : [H^{\frac{1}{2}}(\hat{\Sigma})]^3 \longrightarrow [H^{-\frac{1}{2}}(\hat{\Sigma})]^3,$$

given by

$$\big\langle S_s(\boldsymbol{\gamma}), \boldsymbol{\mu} \big\rangle = \left\langle \mathcal{I}\big(\mathbf{0}, 0, \mathbf{0}, \widehat{\boldsymbol{d}}_s(\boldsymbol{\gamma})\big), \boldsymbol{\mu} \right\rangle,$$

for all $\boldsymbol{\gamma}, \boldsymbol{\mu} \in [H^{\frac{1}{2}}(\hat{\Sigma})]^3$ and where $\widehat{\boldsymbol{d}_s}(\boldsymbol{\gamma})$ is the solution of the Dirichlet solid problem:

$$\mathcal{S}\left(\widehat{\boldsymbol{d}}_s(\boldsymbol{\gamma}), \boldsymbol{\gamma}\right) = 0.$$

From the above definitions, it follows that problem (27) (or (31)) is equivalent to

$$\text{Formulation (II):} \qquad S_f(\boldsymbol{\gamma}) + S_s(\boldsymbol{\gamma}) = 0. \tag{32}$$

The composition of (32) with the inverse operators S_s^{-1} gives rise to the Dirichlet-to-Neumann formulation, namely

$$\text{Formulation (III):} \qquad S_s^{-1}\big(-S_f(\boldsymbol{\gamma})\big) - \boldsymbol{\gamma} = 0. \tag{33}$$

We could also consider the Neumann-to-Dirichlet formulation

$$S_f^{-1}\big(-S_s(\boldsymbol{\gamma})\big) - \boldsymbol{\gamma} = 0$$

by composing (32) with S_f^{-1}. Nevertheless it is rarely used in practice and it is known to lead to poor algorithms in some cases, as pointed out in [8].

5 A partitioned Newton method

In what follows, we skip the upper script n since the time step is fixed. The method presented here consists in solving (31) by a Newton method: given an initial guess $(\widehat{\boldsymbol{u}}_0, \widehat{p}_0, \widehat{\boldsymbol{d}_f}^0, \widehat{\boldsymbol{d}_s}^0, \boldsymbol{\gamma}_0)$, the algorithm reads

1. Evaluate the nonlinear residual of problem (31).
2. Solve the tangent problem (see (37) below) by a domain decomposition method.
3. Update solution:
$$\left(\widehat{\boldsymbol{u}}, \widehat{p}, \widehat{\boldsymbol{d}}_f, \widehat{\boldsymbol{d}}_s, \boldsymbol{\gamma}\right) \leftarrow \left(\widehat{\boldsymbol{u}}, \widehat{p}, \widehat{\boldsymbol{d}}_f, \widehat{\boldsymbol{d}}_s, \boldsymbol{\gamma}\right) + \left(\delta\widehat{\boldsymbol{u}}, \delta\widehat{p}, \delta\widehat{\boldsymbol{d}}_f, \delta\widehat{\boldsymbol{d}}_s, \delta\boldsymbol{\gamma}\right).$$
4. repeat until convergence.

Compared to the known fluid-structure algorithms presented in Section 1.3, this partitioned Newton method amounts to switching the domain decomposition and the linearization in the resolution of the coupled problem. We provide the tangent problem in the following sections, as well as details for the domain decomposition resolution.

5.1 Weak state operators derivatives

In this section, we present the differentiation of the fluid, structure and interface operators of Section 4.2 with respect to their arguments. This derivation uses shape derivative calculus for the differentiation of integral terms with respect to their supports. We refer the reader to [23] where this issue is addressed (see also [16, 4]).

The linearized fluid operator at state $(\widehat{\boldsymbol{u}}, \widehat{p}, \widehat{\boldsymbol{d}}_f, \boldsymbol{\gamma}) \in [H^1(\widehat{\Omega}_f)]^3 \times L^2(\widehat{\Omega}_f) \times [H^1(\widehat{\Omega}_f)]^3 \times [H^{\frac{1}{2}}(\widehat{\Sigma})]^3$ is denoted by

$$\mathrm{D}\,\mathcal{F}(\widehat{\boldsymbol{u}}, \widehat{p}, \widehat{\boldsymbol{d}}_f, \boldsymbol{\gamma}) : [H^1(\widehat{\Omega}_f)]^3 \times L^2(\widehat{\Omega}_f) \times [H^1(\widehat{\Omega}_f)]^3 \times [H^{\frac{1}{2}}(\widehat{\Sigma})]^3 \longrightarrow \left([H^1_{\widehat{\Sigma}}(\widehat{\Omega}_f)]^3 \times L^2(\widehat{\Omega}_f) \times [L^2(\widehat{\Sigma})]^3 \times [L^2(\widehat{\Omega}_f)]^3\right)',$$

and is given by

$$
\begin{aligned}
&\langle \mathrm{D}\,\mathcal{F}(\widehat{\boldsymbol{u}},\widehat{p},\widehat{\boldsymbol{d}}_f,\boldsymbol{\gamma})\cdot(\delta\widehat{\boldsymbol{u}},\delta\widehat{p},\delta\widehat{\boldsymbol{d}_f},\delta\boldsymbol{\gamma}),(\widehat{\boldsymbol{v}_f},\widehat{q},\widehat{\boldsymbol{\xi}},\widehat{\boldsymbol{\tau}})\rangle\\
&=\int_{\Omega_F(\widehat{\boldsymbol{d}_f})}\mathrm{div}\left[\rho_f\delta\boldsymbol{u}\otimes(\boldsymbol{u}^n-\boldsymbol{w}(\widehat{\boldsymbol{d}_f}))\right]\cdot\boldsymbol{v}_f\,\mathrm{d}\boldsymbol{x}\\
&\quad+\int_{\Omega_F(\widehat{\boldsymbol{d}_f})}\boldsymbol{\sigma}(\delta\boldsymbol{u},\delta p):\nabla\boldsymbol{v}_f\,\mathrm{d}\boldsymbol{x}\\
&-\int_{\Omega_F(\widehat{\boldsymbol{d}_f})}q\,\mathrm{div}\,\delta\boldsymbol{u}\,\mathrm{d}\boldsymbol{x}+\frac{1}{\Delta t}\int_{\Omega_F(\widehat{\boldsymbol{d}_f})}(\mathrm{div}\,\delta\widehat{\boldsymbol{d}_f})\rho_f\boldsymbol{u}\cdot\boldsymbol{v}_f\,\mathrm{d}\boldsymbol{x}\\
&+\int_{\Omega_F(\widehat{\boldsymbol{d}_f})}\mathrm{div}\left\{\rho_f\boldsymbol{u}\otimes(\boldsymbol{u}^n-\boldsymbol{w}(\widehat{\boldsymbol{d}_f}))\left[\mathrm{I}\,\mathrm{div}\,\delta\widehat{\boldsymbol{d}_f}-(\nabla\delta\widehat{\boldsymbol{d}_f})^{\mathrm{T}}\right]\right\}\cdot\boldsymbol{v}_f\,\mathrm{d}\boldsymbol{x}\\
&-\frac{1}{\Delta t}\int_{\Omega_F(\widehat{\boldsymbol{d}_f})}\mathrm{div}(\rho_f\boldsymbol{u}\otimes\delta\widehat{\boldsymbol{d}_f})\cdot\boldsymbol{v}_f\,\mathrm{d}\boldsymbol{x}\\
&\quad+\int_{\Omega_F(\widehat{\boldsymbol{d}_f})}\boldsymbol{\sigma}(\boldsymbol{u},p)\left[\mathrm{I}\,\mathrm{div}\,\delta\widehat{\boldsymbol{d}_f}-(\nabla\delta\widehat{\boldsymbol{d}_f})^{\mathrm{T}}\right]:\nabla\boldsymbol{v}_f\,\mathrm{d}\boldsymbol{x}\\
&-\int_{\Omega_F(\widehat{\boldsymbol{d}_f})}\mu\left[\nabla\boldsymbol{u}\nabla\delta\widehat{\boldsymbol{d}_f}+(\nabla\delta\widehat{\boldsymbol{d}_f})^{\mathrm{T}}(\nabla\boldsymbol{u})^{\mathrm{T}}\right]:\nabla\boldsymbol{v}_f\,\mathrm{d}\boldsymbol{x}\\
&-\int_{\Omega_F(\widehat{\boldsymbol{d}_f})}q\,\mathrm{div}\left\{\boldsymbol{u}\left[\mathrm{I}\,\mathrm{div}\,\delta\widehat{\boldsymbol{d}_f}-(\nabla\delta\widehat{\boldsymbol{d}_f})^{\mathrm{T}}\right]\right\}\mathrm{d}\boldsymbol{x}+\int_{\widehat{\Sigma}}\left(\delta\widehat{\boldsymbol{u}}-\frac{\delta\widehat{\boldsymbol{d}_f}}{\Delta t}\right)\cdot\widehat{\boldsymbol{\xi}}\,\mathrm{d}\hat{\boldsymbol{a}}\\
&+\frac{\rho}{\Delta t}\int_{\Omega_F(\widehat{\boldsymbol{d}_f})}\delta\boldsymbol{u}\cdot\boldsymbol{v}_f\,\mathrm{d}\boldsymbol{x}+\int_{\widehat{\Omega}_F}(\delta\widehat{\boldsymbol{d}_f}-\mathrm{Ext}(\delta\boldsymbol{\gamma}))\cdot\widehat{\boldsymbol{\tau}}\,\mathrm{d}\hat{\boldsymbol{x}}
\end{aligned}
\tag{34}
$$

for all $(\widehat{\boldsymbol{v}_f},\widehat{q},\widehat{\boldsymbol{\xi}},\widehat{\boldsymbol{\tau}})\in[H^1(\widehat{\Omega}_f)]^3\times L^2(\widehat{\Omega}_f)\times[L^2(\widehat{\Sigma})]^3\times[L^2(\widehat{\Omega}_f)]^3$.

The linearized solid operator at state $(\widehat{\boldsymbol{d}}_s,\boldsymbol{\gamma})\in[H^1_{\Gamma_D}(\widehat{\Omega}_s)]^3\times[L^2(\widehat{\Sigma})]^3$

$$\mathrm{D}\,\mathcal{S}(\widehat{\boldsymbol{d}}_s,\boldsymbol{\gamma}):[H^1_{\Gamma_D}(\widehat{\Omega}_s)]^3\times[H^{\frac12}(\widehat{\Sigma})]^3\longrightarrow([H^1_{\Gamma_D\cup\widehat{\Sigma}}(\widehat{\Omega}_s)]^3\times[L^2(\widehat{\Sigma})]^3)',$$

is given by

$$
\begin{aligned}
\langle \mathrm{D}\,\mathcal{S}(\widehat{\boldsymbol{d}}_s,\boldsymbol{\gamma})\cdot(\delta\widehat{\boldsymbol{d}_s},\delta\boldsymbol{\gamma}),(\widehat{\boldsymbol{v}_s},\widehat{\boldsymbol{\zeta}})\rangle&=\frac{2}{(\Delta t)^2}\int_{\widehat{\Omega}_S}\rho_0\delta\widehat{\boldsymbol{d}_s}\cdot\boldsymbol{v}_s\,\mathrm{d}\hat{\boldsymbol{x}}\\
&+\frac12\int_{\widehat{\Omega}_S}\nabla\delta\widehat{\boldsymbol{d}_s}:\left(\frac{\partial^2W}{\partial F^2}(I+\nabla\widehat{\boldsymbol{d}_s})\right):\nabla\boldsymbol{v}_s\,\mathrm{d}\hat{\boldsymbol{x}}+\int_{\widehat{\Sigma}}(\delta\widehat{\boldsymbol{d}_s}-\delta\boldsymbol{\gamma})\cdot\widehat{\boldsymbol{\zeta}}\,\mathrm{d}\hat{\boldsymbol{a}},
\end{aligned}
\tag{35}
$$

for all $(\widehat{\boldsymbol{v}_s},\widehat{\boldsymbol{\zeta}})\in[H^1_{\Gamma_D}(\widehat{\Omega}_s)]^3\times[L^2(\widehat{\Sigma})]^3$.

We finally introduce the linearized interface operator at state $(\widehat{\boldsymbol{u}},\widehat{p},\widehat{\boldsymbol{d}}_f,\widehat{\boldsymbol{d}}_s)$

$$\mathrm{D}\,\mathcal{I}(\widehat{\boldsymbol{u}},\widehat{p},\widehat{\boldsymbol{d}}_f,\widehat{\boldsymbol{d}}_s):[H^1(\widehat{\Omega}_f)]^3\times L^2(\widehat{\Omega}_f)\times[H^1(\widehat{\Omega}_f)]^3\times[H^1(\widehat{\Omega}_s)]^3\longrightarrow[H^{-\frac12}(\widehat{\Sigma})]^3,$$

defined by

$$
\begin{aligned}
\left\langle \mathrm{D}\,\mathcal{I}(\widehat{\boldsymbol{u}},\widehat{p},\widehat{\boldsymbol{d}}_f,\widehat{\boldsymbol{d}}_s)\cdot\left(\delta\widehat{\boldsymbol{u}},\delta\widehat{p},\delta\widehat{\boldsymbol{d}}_f,\delta\widehat{\boldsymbol{d}}_s\right),\boldsymbol{\mu}\right\rangle&\\
=\left\langle \mathrm{D}\,\mathcal{F}\left(\widehat{\boldsymbol{u}},\widehat{p},\widehat{\boldsymbol{d}}_f,\boldsymbol{0}\right)\cdot\left(\delta\widehat{\boldsymbol{u}},\delta\widehat{p},\delta\widehat{\boldsymbol{d}}_f,\boldsymbol{0}\right),(\mathcal{L}_f\boldsymbol{\mu},0,\boldsymbol{0},\boldsymbol{0})\right\rangle&\\
+\left\langle \mathrm{D}\,\mathcal{S}\left(\widehat{\boldsymbol{d}}_s,\boldsymbol{0}\right)\left(\delta\widehat{\boldsymbol{d}}_s,\boldsymbol{0}\right),(\mathcal{L}_s\boldsymbol{\mu},\boldsymbol{0})\right\rangle,&
\end{aligned}
\tag{36}
$$

for all $\boldsymbol{\mu} \in [H^{\frac{1}{2}}(\widehat{\Sigma})]^3$.

In terms of the operators defined above, the tangent problem associated with (31) reads

$$\begin{cases} \mathrm{D}\,\mathcal{F}\left(\widehat{\boldsymbol{u}}, \widehat{p}, \widehat{\boldsymbol{d}}_f, \boldsymbol{\gamma}\right) \cdot \left(\delta\widehat{\boldsymbol{u}}, \delta\widehat{p}, \delta\widehat{\boldsymbol{d}}_f, \delta\boldsymbol{\gamma}\right) = -\mathcal{F}\left(\widehat{\boldsymbol{u}}, \widehat{p}, \widehat{\boldsymbol{d}}_f, \boldsymbol{\gamma}\right), \\ \mathrm{D}\,\mathcal{S}\left(\widehat{\boldsymbol{d}}_s, \boldsymbol{\gamma}\right) \cdot \left(\delta\widehat{\boldsymbol{d}}_s, \delta\boldsymbol{\gamma}\right) = -\mathcal{S}\left(\widehat{\boldsymbol{d}}_s, \boldsymbol{\gamma}\right), \\ \mathrm{D}\,\mathcal{I}\left(\widehat{\boldsymbol{u}}, \widehat{p}, \widehat{\boldsymbol{d}}_f, \widehat{\boldsymbol{d}}_s\right) \cdot \left(\delta\widehat{\boldsymbol{u}}, \delta\widehat{p}, \delta\widehat{\boldsymbol{d}}_f, \delta\widehat{\boldsymbol{d}}_s\right) = -\mathcal{I}\left(\widehat{\boldsymbol{u}}, \widehat{p}, \widehat{\boldsymbol{d}}_f, \widehat{\boldsymbol{d}}_s\right). \end{cases} \tag{37}$$

Once the linear fluid, solid and interface operators $\mathrm{D}\,\mathcal{F}$, $\mathrm{D}\,\mathcal{S}$ and $\mathrm{D}\,\mathcal{I}$ are defined, we can introduce the linear Steklov-Poincaré operators $S_{F,l}$ and $S_{S,l}$ using the formula of Section 4.3 with the linearized operators instead of the nonlinear operators. It may be noticed that the linear Steklov-Poincaré operators are different from the linearization of the nonlinear Steklov operators of Section 4.3.

5.2 Implementation issues

In this subsection, we briefly describe the general domain decomposition algorithm used to solve the linear problems introduced above, namely both the Dirichlet-Neumann and the Neumann-Neumann algorithms (in Table 1).

General algorithm.

Following the practical implementation, we decompose the algorithm according to three distinct solvers: the master (which, roughly speaking, solves the third equation of (37) by a GMRES method), the fluid solver (which solves the first equation of (37)) and the solid solver (which solves the second equation of (37)).

The iterative algorithm is as follows:

1. Evaluate the Newton residual (right-hand sides of (37)).
2. Initialization of the Domain Decomposition method:
   (a) Lifting of the external load and boundary conditions, that is solve the first and second equations of (37) with $\delta\boldsymbol{\gamma} = 0$.
   (b) Computation of the right-hand side of the Schur complement by the master, insert the residuals received from the fluid and from the solid into (36) and the third equation of (37). This step evaluates how far the solution with zero on the interface is from the true solution of the coupled problem (37).
   (c) Preconditioning the right-hand side of the Schur complement.
3. Iteration until convergence of the GMRES algorithm on the Schur complement by the master, which updates the displacement $\delta\boldsymbol{\gamma}$, sends it to the fluid and solid solvers in order to
   (a) Evaluate the new residual
   (b) Preconditioning the residual

4. End of the domain decomposition algorithm.

The detailed description of these steps for both the Dirichlet-Neumann and Neumann-Neumann algorithms is given in Table 1, which is commented in the following two paragraphs. Note that the steps (2a) and (4) do not depend on the preconditioner.

Dirichlet-Neumann preconditioner

The Dirichlet-Neumann preconditioner amounts to preconditioning the Schur complement using the solid problem only, namely the exact tangent problem of the solid (second equation of (37)) with Neumann boundary conditions. It is worth noticing that the preconditioning step is not performed in parallel since only the structure problem is used to precondition the residual. For each iteration (3) of the GMRES algorithm on the Schur complement, the master sends $\delta\boldsymbol{\gamma}$ in Step (3a) to the fluid solver only, which performs the instructions of Table 1 and returns a residual to the master. In Step (3b), the master sends this residual to the solid solver, which applies the preconditioner according to Table 1 and returns a displacement $\delta\tilde{\boldsymbol{\gamma}}$. The master then sums the displacements $\frac{1}{2}(\delta\boldsymbol{\gamma} + \delta\tilde{\boldsymbol{\gamma}})$ and computes a new displacement using the update formula of the GMRES algorithm. At convergence, the final value of $\delta\boldsymbol{\gamma}$ is known and the solutions in the fluid and in the solid are computed as indicated in Table 1.

Let us point out that the Dirichlet-Neumann algorithm described above is a purely sequential algorithm.

Neumann-Neumann preconditioner

The Neumann-Neumann preconditioner uses both the tangent fluid problem and the tangent solid problem (first and second equations of (37)) with Neumann boundary conditions. This algorithm is fully parallel since both the preconditioning steps (2c) and (3b) and residual evaluation steps (3a) can be done simultaneously by the fluid and solid solvers. Although for the tangent solid problem, considering Neumann boundary conditions is standard, for the tangent fluid problem this is not the case. In particular, shape derivative terms (that depend on the lifting $\boldsymbol{w}(\delta\widehat{\boldsymbol{d}}_f)$ of the fluid domain displacement, and thus on the solution $\delta\widehat{\boldsymbol{d}}_f$ itself on the interface) enter the stiffness matrix of (34) when Neumann boundary conditions are considered. Yet, the lifting matrix of (17) is never constructed and neither is the fluid tangent matrix. Therefore, each iteration of the GMRES algorithm to solve the tangent fluid problem requires the full solution of (17) by a GMRES algorithm. In practical implementation, it is easier and less expensive to neglect the shape derivatives terms in (34). Doing so, we slightly modify the classical Neumann-Neumann preconditioner.

Some remarks on the stopping criteria

In the above described algorithms, a Newton method is combined with a linear solver (which uses the domain decomposition methods). There are thus at least two parameters to be fixed: the stopping criterium for the Newton algorithm and the stopping criterium for the linear solvers using iterative algorithms (such as GMRES). Based on the principle that the overall stopping criterium

Steps	Dirichlet-Neumann		Neumann-Neumann	
	Solid	Fluid	Solid	Fluid
(2a), (4)	Receive $\delta\boldsymbol{\gamma}$	Receive $\delta\boldsymbol{\gamma}$	Receive $\delta\boldsymbol{\gamma}$	Receive $\delta\boldsymbol{\gamma}$
	Matrix construction^c Matrix factorization^c (Dirichlet) Forward backward substitution (with external BC^a and displacement on the interface)	Computation of a preconditionner^c (in the fluid subdomain) GMRES (with external BC^a and velocity^b on the interface)	Matrix construction^c Matrix factorization^c (Dirichlet) Forward backward substitution (with external BC^a and displacement on the interface)	Computation of a preconditionner^c (in the fluid subdomain) GMRES (with external BC^a and velocity^b on the interface)
	Send linear residual	Send linear residual	Send linear residual	Send linear residual
(2c),(3b)	Receive residual		Receive residual	Receive residual
	Matrix factorization^d (Neumann) Forward backward substitution		Matrix factorization^d (Neumann) Forward backward substitution	Computation of a preconditioner^d (in the fluid subdomain) GMRES
	Send linear displacement		Send linear displacement	Send linear displacement
(3a)		Receive displacement	Receive displacement	Receive displacement
		GMRES	Forward backward substitution	GMRES
		Send linear residual	Send linear residual	Send linear residual

Table 1: Detailed description of the algorithm

will be driven by the Newton algorithm, it is not necessary to "over-solve" the linear problems (especially the tangent fluid problem). Thus there is a non trivial interplay between the tolerance of the Newton algorithm and the tolerance of the GMRES algorithm, that may change significantly the efficiency of the algorithms.

5.3 Complexity analysis

Let us make a formal complexity analysis to have a rough hint on the cost of the Steklov type, Dirichlet to Neumann formulation based, and partitioned Newton type methods. We make the following assumptions: the fluid to be solved at each time step is linear (*e.g.* semi-implicit Euler scheme for Navier-Stokes equations), the structure problem is solved by a Newton algorithm and the linearized structure problems by direct methods. We only take into account the factorization for the resolution of the structure sub-problem and consider the matrices as already factorized when dealing with linear domain decomposition methods.

In the following analysis we assume that the number of Newton iterations, $\widetilde{Ne_{FSI}}$, for the global problem in formulations (II) and (III) is the same. Let Ne_{FSI} the number of Newton iterations for the formulation (I). We denote by Ne_s the number of iterations for a Newton algorithm in the structure problem. The number of GMRES iterations G is assumed not to depend on the algorithm if optimal preconditioners (let say Dirichlet-Neumann) are used. In the sequel Cr and Fa denote respectively the cost of the construction and factorization a matrix in the solid, Fl_1 the resolution cost per time step of the fluid problem, and Fl_2 the resolution cost for a tangent fluid problem. The estimations of costs for the three types of methods are gathered in Table 2 both for a sequential and a parallel implementation when possible. For the parallel implementation, we have assumed that $Fa + Cr \geq Fl$ and $Fl \geq Fa$.

Method	(I) NtoD preconditioned partitioned Newton	(II) NtoD preconditioned Newton on Steklov	(III) Newton on DtoN-formulation
Sequential	$Ne_{FSI}\,[2Fa + Cr$ $+GFl_2 + Fl_1]$	$\widetilde{Ne_{FSI}}\,[(Ne_s + 1)(Fa + Cr)$ $+Fa + GFl_2 + Fl_1]$	$\widetilde{Ne_{FSI}}\,[(Ne_s + 1)(Fa + Cr)$ $+Fl_1 + GFl_2]$
Parallel	$Ne_{FSI}\,[2Fa + Cr$ $+GFl_2]$	$Ne_{FSI}\,[(Ne_s + 1)(Fa + Cr)$ $+Fa + GFl_2]$	-

Table 2: Estimation of the computational cost

Let us comment on Table 2. For the sequential implementation the estimations for the method (II) and (III) only differ by the factorization cost of a solid tangent matrix, which is rather small with respect to the whole cost. This is in agreement with the tests performed in [14] where method (II) is shown to be roughly equivalent to method (III) in terms of cost. If $Ne_{FSI} \approx \widetilde{Ne_{FSI}}$, method (I) should be at least as efficient as the first two, especially if the structure is nonlinear and expensive. On the contrary, if $Fl \geq Fa + Cr$ then the parallel implementations of methods (I) and (II) seem to be completely equivalent in terms of cost, which is only determined by the fluid. For the parallel implementation, the cost reduction strongly depends on the number of GMRES

iterations, and the method (I) still seems to compete with method (II). Note that, if $Ne_{FSI} > \widetilde{Ne_{FSI}}$, method (I) may loss efficiency with respect to methods (II) and (III).

The condition $Fa+Cr \geq Fl$ is almost never satisfied if classical shell elements are used. However, this condition may be satisfied when 3D shell elements are used to model more realistic constitutive laws for the structure (see Section 3). Let consider for instance a mesh with 38000 nodes in the fluid (let say 150000 degrees of freedom). For MITC4 shell elements, we then have 3300 nodes and 16500 degrees of freedom. Numerical tests show that in this case, with the same computer, $Fl \simeq 45s$, $Fa \simeq 0.7s$ and $Cr \simeq 1.7s$. Let now consider 3D shell elements (hexahedra, 27 nodes per element) on the same mesh. The number of nodes for the structure increases from 3300 to 22100, and the number of degrees of freedom from 16500 to 66300. The costs for the solid are now $Fa \simeq 13s$ and $Cr \simeq 50s$. We are thus in the situation $Cr + Fa \geq Fl$ and $Fl \geq Fa$.

6 Numerical tests

In this section we illustrate the behavior of the linear Domain Decomposition method (I), with a Dirichlet-Neumann preconditioner, by performing some numerical simulations. As regards efficiency, we make some comparisons with the nonlinear Domain Decomposition method (III), reported in [23].

In all the computations the structure is modeled by 3D-shell elements, as reported in §3.2, with a neo-Hookean constitutive law in finite deformation. For the space discretization we use a $\mathbb{Q}_2$-finite element (27 nodes) combined with a MITC interpolation rule in the thin direction of the hexaedra. This allow us to deal with three dimensional constitutive laws while keeping a reasonable cost (only one layer of elements is necessary). A mid-point rule is used for the time discretization. For the fluid, we consider the Navier-Stokes equation with an ALE formulation (11). The fluid equations are discretized in space using $\mathbb{P}_1/\mathbb{P}_1$-SUPG-stabilized finite elements, and in time by a semi-implicit backward-Euler scheme.

6.1 Flow in a compliant straight vessel

We consider here the benchmark reported in [24]. The fluid computational domain is a cylinder of radius $R_0 = 0.5\,cm$ and of length $L = 5\,cm$. The vessel wall has a thickness of $h = 0.1\,cm$ and the rest of physical parameters are $E = 3 \cdot 10^6\,dynes/cm^2$, $\nu = 0.3$ and $\rho_s = 1.2\,g/cm^3$. For the fluid we have $\mu = 0.035\,poise$ and $\rho_f = 1\,g/cm^2$. The numerical computations are performed using a fluid mesh with 38400 tetrahedra and a solid mesh with 160 hexahedra, the time step size is $\Delta t = 10^{-4}\,s$.

Initially, the fluid is at rest and an over pressure of $1.3332 \cdot 10^4\,dynes/cm^2$ ($10\,mmHg$) is been imposed at the inlet boundary during $0.005\,s$. As expected, a pressure wave propagation is observed, see Figure 3. This results are comparable with those obtained with more standard shell elements (see *e.g.* [26, 19] with the MITC4 shell element).

The same numerical computation have been carried out using method (III). A comparison of the efficiency of both methods is reported on Table 3. We

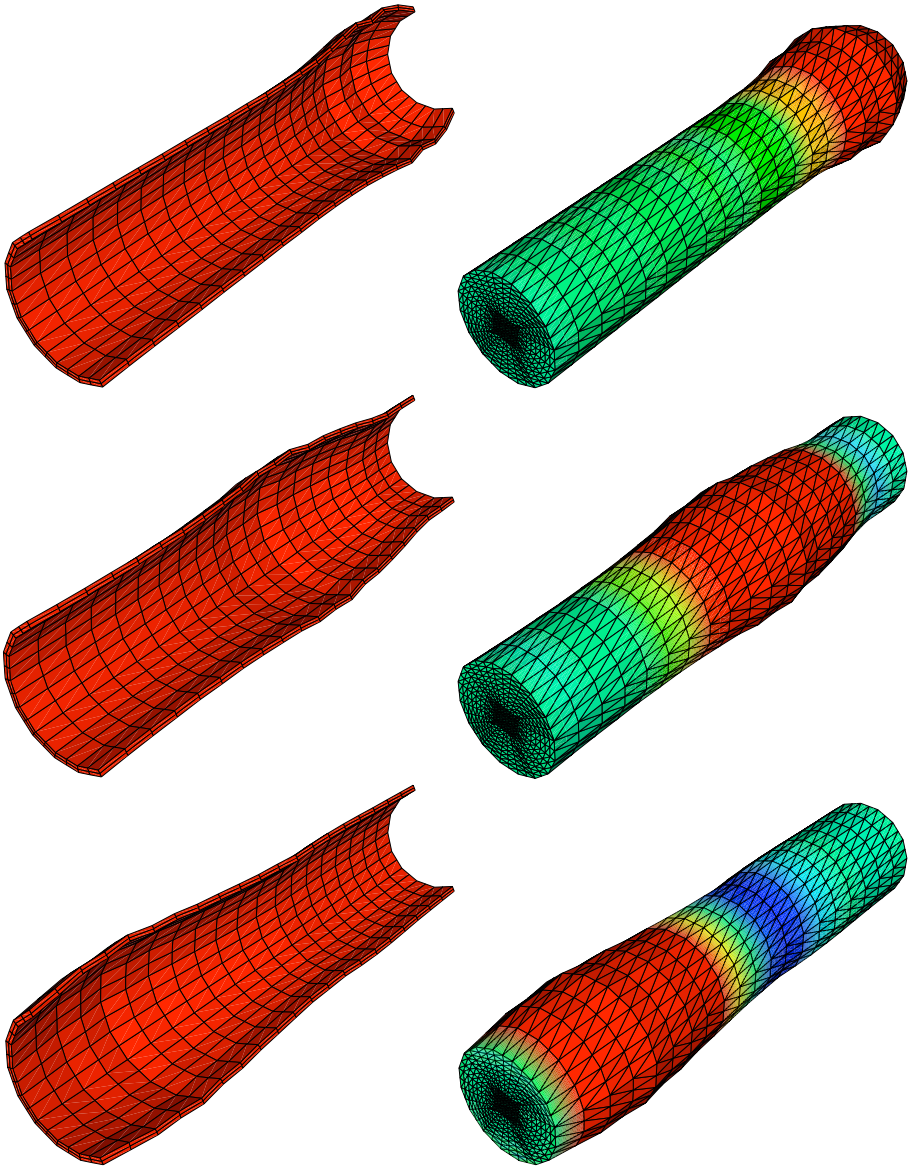

Figure 3: Deformation of the structure (left), magnified by 5, and fluid pressure at time 4, 8 and 13 ms. Note that the structure is made of one layer of 3D-shell elements.

observe that method (III) is slightly faster than method (I), mainly due to the reduced number of Newton iterations.

Method	(I)	(III)
CPU time (dimensionless)	1	0.7
Average number of GMRES iterations	7	10
Average number of Newton iterations	5	2

Table 3: Efficiency over 10 time steps

6.2 Flow in a compliant vessel with an aneurysm

We consider now the FSI numerical results reported in [43] using *in vitro* aneurysm geometries. The fluid computational domain is the idealized abdominal aortic aneurysm given in Figure 4. The geometry models a middle-size aneurysm with a dilatation ratio $D/d = 2.4$ (maximum diameter to inlet diameter ratio) and aspect ratio $L/d = 3.9$ (length to inlet diameter ratio), with $d = 1.7\,cm$ (we refer to [43, 44] for the details). The vessel wall has a uniform thickness of $h = 0.17\,cm$ and the physical parameters are given by $E = 6 \cdot 10^6\,dynes/cm^2$, $\nu = 0.3$ and $\rho_s = 1.2\,g/cm^3$. For the fluid we have $\mu = 0.035\,poise$ and $\rho_f = 1\,g/cm^2$. The fluid and solid meshes are made of 165888 tetrahedra and 640 hexahedra, respectively. The time step size is $\Delta t = 1.68 \times 10^{-3}\,s$.

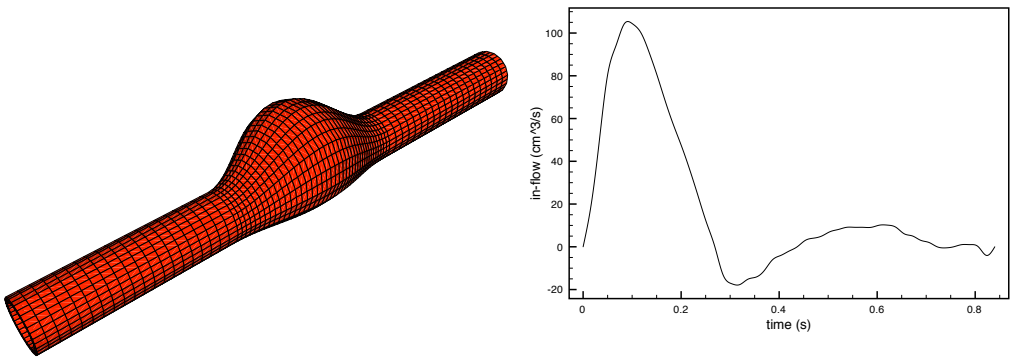

Figure 4: Aneurysm geometry (left) and in-flow rate data (right)

Initially, the fluid is at rest. The in-flow rate corresponding to a cardiac cycle, see Figure 4(right), is imposed on the inlet boundary. A resistive-like boundary condition is prescribed on the outlet boundary, the value of the resistance being $R = 3 \times 10^3\,dyne/cm^3$. In Figure 5 we have reported some snapshots of the wall deformation and the fluid velocity field at different time instants. This results are in agreement with those obtained with the MITC4 shell element in [43].

As in the previous experiment, the same numerical simulation have been performed using method (III). A comparison of the efficiency is reported on

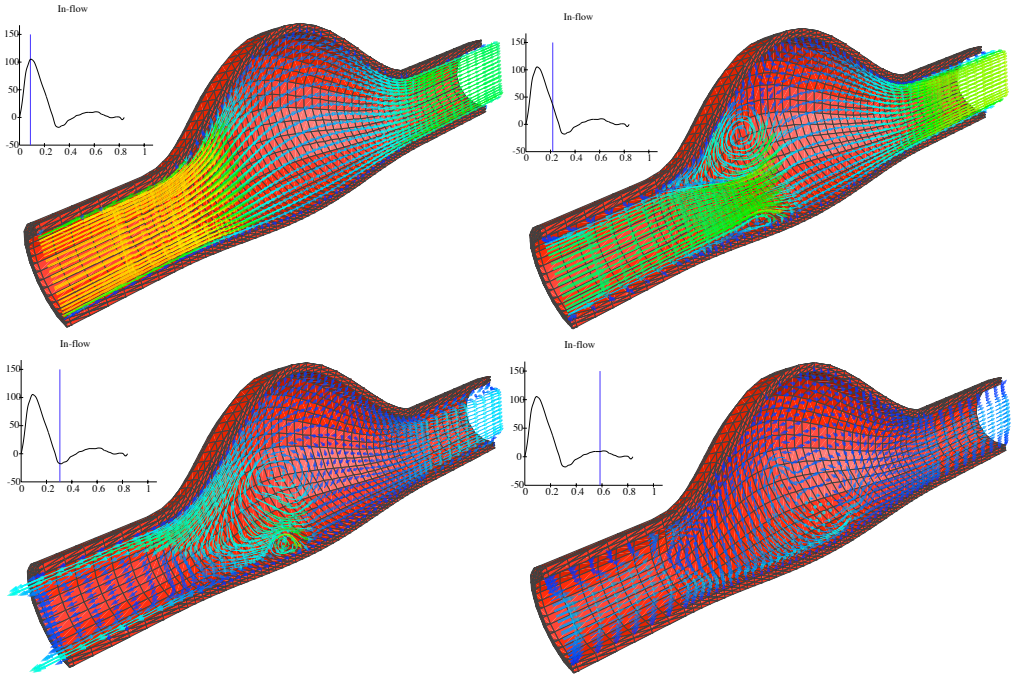

Figure 5: Deformation of the structure and fluid velocity field at time 87.36×10^{-3}, 218.4×10^{-3}, 305.76×10^{-3} and $584.64 \times 10^{-3} s$.

Table 4. Once again, method (III) performs slightly faster. Nevertheless, we can notice that the efficiency gap between both methods (see Table 3) has been reduced, due to the increasing in the computational cost of the structural solver.

Method	(I)	(III)
CPU time (dimensionless)	1	0.8
Average number of GMRES iterations	7	10
Average number of Newton iterations	6	3

Table 4: Efficiency over 10 time steps

7 Conclusion

We have proposed a Newton algorithm for fluid-structure problems. The starting point of the method is the same as for the so-called monolithic approaches since we consider the global fluid-structure equations, but the tangent problem is solved with domain decomposition techniques.

The resulting method is therefore partitioned: it is based on two different solvers for the fluid and the structures and can be parallelized. In this way,

the proposed approach overcomes one of the main drawbacks of the standard monolithic schemes used in fluid-structure interaction.

As regards efficiency, a simplified complexity analysis showed that the proposed scheme is expected to reach optimal performance when the structure and fluid solvers are very expensive, provided that the global number of Newton iterations is of the same order. In spite of that, the numerical results reported in this paper showed that the proposed approaches do not outperform some classical partitioned Newton procedures in which the domain decomposition framework is applied at the nonlinear level [26, 23, 14]. This information should be taken into consideration by those interested in developing a monolothic fluid-structure interaction solver.

References

[1] S. Badia, F. Nobile, and C. Vergara. Fluid-structure partitioned procedures based on Robin transmission conditions. *J. Comp. Phys.*, 227:7027–7051, 2008.

[2] K.J. Bathe and H. Zhang. Finite element developments for general fluid flows with structural interactions. *Int. J. Num. Meth. Engng.*, 2004.

[3] J.T. Batina. Unsteady Euler airfoil solutions using unstructured dynamic meshes. *AIAA J.*, 28(8):1381–1388, 1990.

[4] Y. Bazilevs, V.M. Calo, T.J.R. Hughes, and Y. Zhang. Isogeometric fluid-structure interaction: Theory, algorithms, and computations. Technical Report 08-16, ICES, 2008.

[5] Y. Bazilevs, V.M. Calo, Y. Zhang, and T.J.R. Hughes. Isogeometric fluid-structure interaction analysis with applications to arterial blood flow. *Comput. Mech.*, 38:310–322, 2006.

[6] E. Burman and M.A. Fernández. Stabilized explicit coupling for fluid-structure interaction using Nitsche's method. *C. R. Math. Acad. Sci. Paris*, 345(8):467–472, 2007.

[7] D. Caillerie, A. Mourad, and Raoult A. Cell-to-muscle homogenization. Application to a constitutive law for the myocardium. *Math. Model. Num. Anal.*, 37:681–698, 2003.

[8] P. Causin, J.-F. Gerbeau, and F. Nobile. Added-mass effect in the design of partitioned algorithms for fluid-structure problems. *Comp. Meth. Appl. Mech. Engng.*, 194(42–44):4506–4527, 2005.

[9] D. Chapelle and K.J. Bathe. *The Finite Element Analysis of Shells - Fundamentals*. Springer Verlag, 2003.

[10] D. Chapelle and A. Ferent. Modeling of the inclusion of a reinforcing sheet within a 3D medium. *Math. Models Methods Appl. Sci.*, 13(4):573–595, 2003.

[11] D. Chapelle, A. Ferent, and K.J. Bathe. 3D-shell elements and their underlying mathematical model. *Math. Models Methods Appl. Sci.*, 14(1):105–142, 2004.

[12] D. Chapelle, A. Ferent, and P. Le Tallec. The treatment of "pinching locking" in 3D-shell elements. *M2AN Math. Model. Numer. Anal.*, 37(1):143–158, 2003.

[13] S. Deparis. *Numerical Analysis of Axisymmetric Flows and Methods for Fluid-Structure Interaction Arising in Blood Flow Simulation*. PhD thesis, EPFL, Switzerland, 2004.

[14] S. Deparis, M. Discacciati, G. Fourestey, and A. Quarteroni. Fluid-structure algorithms based on Steklov-Poincaré operators. *Comput. Methods Appl. Mech. Engrg.*, 195(41-43):5797–5812, 2006.

[15] S. Deparis, M. Discacciati, and A. Quarteroni. A domain decomposition framework for fluid-structure interaction problems. In *Proceedings of the Third International Conference on Computational Fluid Dynamics (ICCFD3)*, 2004.

[16] W. Dettmer and D. Perić. A computational framework for fluid-structure interaction: Finite element formulation and applications. *Comp. Meth. Appl. Mech. Engrg.*, 195(41-43):5754–5779, 2006.

[17] J. Donéa, S. Giuliani, and J. P. Halleux. An arbitrary Lagrangian-Eulerian finite element method for transient dynamic fluid-structure interactions. *Comp. Meth. Appl. Mech. Engng.*, pages 689–723, 1982.

[18] C. Farhat, K. van der Zee, and Ph. Geuzaine. Provably second-order time-accurate loosely-coupled solution algorithms for transient nonlinear aeroelasticity. *Comp. Meth. Appl. Mech. Engng.*, 195(17-18):1973–2001, 2006.

[19] M.A. Fernández, J.-F. Gerbeau, and C. Grandmont. A projection algorithm for fluid-structure interaction problems with strong added-mass effect. *C. R. Acad. Sci. Paris, Math.*, 342:279–284, 2006.

[20] M.A. Fernández, J.-F. Gerbeau, and C. Grandmont. A projection semi-implicit scheme for the coupling of an elastic structure with an incompressible fluid. Int. J. Num. Meth. Engng. in press, 2006.

[21] M.A. Fernández and M. Moubachir. An exact block-Newton algorithm for solving fluid-structure interaction problems. *C. R. Math. Acad. Sci. Paris*, 336(8):681–686, 2003.

[22] M.A. Fernández and M. Moubachir. An exact block-newton algorithm for the solution of implicit time discretized coupled systems involved in fluid-structure interaction problems. In K.J. Bathe, editor, *Second M.I.T. Conference on Computational Fluid and Solid Mechanics*, pages 1337–1341. Elsevier, 2003.

[23] M.A. Fernández and M. Moubachir. A Newton method using exact Jacobians for solving fluid-structure coupling. *Comp. & Struct.*, 83:127–142, 2005.

[24] L. Formaggia, J.-F. Gerbeau, F. Nobile, and A. Quarteroni. On the coupling of 3D and 1D Navier-Stokes equations for flow problems in compliant vessels. *Comp. Meth. Appl. Mech. Engrg.*, 191(6-7):561–582, 2001.

[25] Y.C. Fung, K. Fronek, and P. Patitucci. Pseudoelasticity of arteries and the choice of its mathematical expression. *Am. J. Physiol.*, 237:620–631, 1979.

[26] J.-F. Gerbeau and M. Vidrascu. A quasi-Newton algorithm based on a reduced model for fluid-structure interactions problems in blood flows. *Math. Model. Num. Anal.*, 37(4):631–648, 2003.

[27] J.-F. Gerbeau, M. Vidrascu, and P. Frey. Fluid-structure interaction in blood flows on geometries based on medical imaging. *Comp. & Struct.*, 83(2-3):155–165, 2005.

[28] M. Heil. An efficient solver for the fully coupled solution of large-displacement fluid-structure interaction problems. *Comput. Methods Appl. Mech. Engrg.*, 193(1-2):1–23, 2004.

[29] A.H. Holzapfel, T.C. Gasser, and Ogden R.W. A new constitutive framework for arterial wall mechanics and a comparative study of material models. *J. Elasticity*, 61:1–48, 2000.

[30] B. Hübner, E. Walhorn, and D. Dinkle. A monolithic approach to fluid-structure interaction using space-time finite elements. *Comp. Meth. Appl. Mech. Engng.*, 193:2087–2104, 2004.

[31] U. Küttler and W.A. Wall. Fixed-point fluid-structure interaction solvers with dynamic relaxation. *Comput. Mech.*, 2008. DOI 10.1007/s00466-008-0255-5.

[32] P. Le Tallec. Domain decomposition methods in computational mechanics. In *Computational Mechanics Advances, Vol. 1, no.2*, pages 123–217. North Holland, 1994.

[33] P. Le Tallec and J. Mouro. Fluid structure interaction with large structural displacements. *Comput. Meth. Appl. Mech. Engrg.*, 190:3039–3067, 2001.

[34] H.G. Matthies and J. Steindorf. Partitioned but strongly coupled iteration schemes for nonlinear fluid-structure interaction. *Comp. & Struct.*, 80(27–30):1991–1999, 2002.

[35] H.G. Matthies and J. Steindorf. Partitioned strong coupling algorithms for fluid-structure interaction. *Comp. & Struct.*, 81:805–812, 2003.

[36] D. P. Mok and W. A. Wall. Partitioned analysis schemes for the transient interaction of incompressible flows and nonlinear flexible structures. In K. Schweizerhof W.A. Wall, K.U. Bletzinger, editor, *Trends in computational structural mechanics*, Barcelona, 2001. CIMNE.

[37] D. P. Mok, W. A. Wall, and E. Ramm. Partitioned analysis approach for the transient, coupled response of viscous fluids and flexible structures. In W. Wunderlich, editor, *Proceedings of the European Conference on Computational Mechanics*. ECCM'99, TU Munich, 1999.

[38] D. P. Mok, W. A. Wall, and E. Ramm. Accelerated iterative substructuring schemes for instationary fluid-structure interaction. In K.J. Bathe, editor, *Computational Fluid and Solid Mechanics*, pages 1325–1328. Elsevier, 2001.

[39] F. Nobile. *Numerical approximation of fluid-structure interaction problems with application to haemodynamics*. PhD thesis, EPFL, Switzerland, 2001.

[40] Christiaan H.G.A. van Oijen. *Mechanics and design of fiber-reinforced vascular prostheses*. PhD thesis, Technische Universiteit Eindhoven, 2003.

[41] S. Piperno, C. Farhat, and B. Larrouturou. Partitioned procedures for the transient solution of coupled aeroelastic problems. Part I: Model problem, theory and two-dimensional application. *Comp. Meth. Appl. Mech. Engrg.*, 124:79–112, 1995.

[42] S. Rugonyi and K.J. Bathe. On finite element analysis of fluid flows coupled with structural interaction. *CMES - Comp. Modeling Eng. Sci.*, 2(2):195–212, 2001.

[43] A.-V. Salsac, M.A. Fernández, J.M. Chomaz, and P. Le Tallec. Effects of the flexibility of the arterial wall on the wall shear stresses and wall tension in abdominal aortic aneurysms. In *Bulletin of the American Physical Society*, 2005.

[44] A.-V. Salsac, S.R. Sparks, J.M. Chomaz, and J.C. Lasheras. Evolution of the wall shear stresses during the progressive enlargement of symmetric abdominal aortic aneurysms. *J. Fluid Mech.*, 550:19–51, 2006.

[45] T.E. Tezduyar. Finite element methods for fluid dynamics with moving boundaries and interfaces. *Arch. Comput. Methods Engrg.*, 8:83–130, 2001.

[46] P.D. Thomas and C.K. Lombard. Geometric conservation law and its application to flow computations on moving grids. *AIAA J.*, 17(10):1030–1037, 1979.

[47] J. Vierendeels. Implicit coupling of partioned fluid-structure interaction solvers using reduced order models. In M. Schäfer H.J. Bungartz, editor, *Fluid-Structure interaction, Modelling, Simulation, Optimization*, pages 1–18. Springer, 2006.

[48] H. Zhang, X. Zhang, S. Ji, G. Guo, Y. Ledezma, N. Elabbasi, and H. deCougny. Recent development of fluid-structure interaction capabilities in the ADINA system. *Computers & Structures*, 81(8-11):1071–1085, 2003.

Centre de recherche INRIA Paris – Rocquencourt
Domaine de Voluceau - Rocquencourt - BP 105 - 78153 Le Chesnay Cedex (France)

Centre de recherche INRIA Bordeaux – Sud Ouest : Domaine Universitaire - 351, cours de la Libération - 33405 Talence Cedex
Centre de recherche INRIA Grenoble – Rhône-Alpes : 655, avenue de l'Europe - 38334 Montbonnot Saint-Ismier
Centre de recherche INRIA Lille – Nord Europe : Parc Scientifique de la Haute Borne - 40, avenue Halley - 59650 Villeneuve d'Ascq
Centre de recherche INRIA Nancy – Grand Est : LORIA, Technopôle de Nancy-Brabois - Campus scientifique
615, rue du Jardin Botanique - BP 101 - 54602 Villers-lès-Nancy Cedex
Centre de recherche INRIA Rennes – Bretagne Atlantique : IRISA, Campus universitaire de Beaulieu - 35042 Rennes Cedex
Centre de recherche INRIA Saclay – Île-de-France : Parc Orsay Université - ZAC des Vignes : 4, rue Jacques Monod - 91893 Orsay Cedex
Centre de recherche INRIA Sophia Antipolis – Méditerranée : 2004, route des Lucioles - BP 93 - 06902 Sophia Antipolis Cedex

Éditeur
INRIA - Domaine de Voluceau - Rocquencourt, BP 105 - 78153 Le Chesnay Cedex (France)
http://www.inria.fr
ISSN 0249-6399